Contrib Mineral Petrol (2016) 171:92
DOI 10.1007/s00410-016-1297-x

ORIGINAL PAPER

# Oxygen isotope evolution of the Lake Owyhee volcanic field, Oregon, and implications for the low-$\delta^{18}O$ magmatism of the Snake River Plain–Yellowstone hotspot and other low-$\delta^{18}O$ large igneous provinces

**Tyler B. Blum[1] · Kouki Kitajima[1] · Daisuke Nakashima[1,2] · Ariel Strickland[1] · Michael J. Spicuzza[1] · John W. Valley[1]**

Received: 22 April 2016 / Accepted: 2 September 2016


**Abstract** The Snake River Plain–Yellowstone (SRP-Y) hotspot track represents the largest known low-$\delta^{18}O$ igneous province; however, debate persists regarding the timing and distribution of meteoric hydrothermal alteration and subsequent melting/assimilation relative to hotspot magmatism. To further constrain alteration relations for SRP-Y low-$\delta^{18}O$ magmatism, we present in situ $\delta^{18}O$ and U–Pb analyses of zircon, and laser fluorination $\delta^{18}O$ analyses of phenocrysts, from the Lake Owyhee volcanic field (LOVF) of east-central Oregon. U–Pb data place LOVF magmatism between 16.3 and 15.4 Ma, and contain no evidence for xenocrystic zircon. LOVF $\delta^{18}O$(Zrc) values demonstrate (1) both low-$\delta^{18}O$ and high-$\delta^{18}O$ caldera-forming and pre-/post-caldera magmas, (2) relative increases in $\delta^{18}O$ between low-$\delta^{18}O$ caldera-forming and post-caldera units, and (3) low-$\delta^{18}O$ magmatism associated with extension of the Oregon-Idaho Graben. The new data, along with new compilations of (1) in situ zircon $\delta^{18}O$ data for the SRP-Y, and (2) regional $\delta^{18}O$(WR) and $\delta^{18}O$(magma) patterns, further constrain the thermal and structural associations for hydrothermal alteration in the SRP-Y. Models for low-$\delta^{18}O$ magmatism must be compatible with (1) $\delta^{18}O$(magma) trends within individual SRP-Y eruptive centers, (2) along axis trends in $\delta^{18}O$(magma), and (3) the high concentration of low-$\delta^{18}O$ magmas relative to the surrounding regions. When considered with the structural and thermal evolution of the SRP-Y, these constraints support low-$\delta^{18}O$ magma genesis originating from syn-hotspot meteoric hydrothermal alteration, driven by hotspot-derived thermal fluxes superimposed on extensional tectonics. This model is not restricted to continental hotspot settings and may apply to several other low-$\delta^{18}O$ igneous provinces with similar thermal and structural associations.

**Keywords** Oxygen isotopes · Low-$\delta^{18}O$ magmas · Lake Owyhee volcanic field · Snake River Plain–Yellowstone hotspot · Zircon · Large igneous province

## Introduction

The time-transgressive volcanism of the Snake River Plain–Yellowstone (SRP-Y) large igneous province (Fig. 1) forms the largest known low-$\delta^{18}O$ magmatic province on Earth, and remains a source of geochemical and geophysical interest due to the large volume of silicic volcanism, and the current locus of magmatism in the Yellowstone volcanic field. The large volume of low-$\delta^{18}O$ felsic magmas in the SRP-Y contrasts with their relatively limited occurrence globally (Taylor 1986). Decreases in $\delta^{18}O$(WR) from mantle-like values require direct or indirect oxygen exchange with low-$\delta^{18}O$ surface waters at high temperature, which is in part limited by the depths to which significant volumes of meteoric water can circulate. *Magmatic* low-$\delta^{18}O$ values ($\delta^{18}O$(rhyolite) <6.0 ‰) record the assimilation or melting of low-$\delta^{18}O$ rock (Taylor and Sheppard 1986; Bindeman et al. 2004; Bindeman 2008). Since Friedman et al. (1974) first described low-$^{18}O/^{16}O$ ratios

Communicated by Jochen Hoefs.

**Electronic supplementary material** The online version of this article (doi:10.1007/s00410-016-1297-x) contains supplementary material, which is available to authorized users.

✉ Tyler B. Blum
tbblum@geology.wisc.edu

[1] Department of Geoscience, University of Wisconsin-Madison, Madison, WI 53706, USA

[2] Tohoku University, Miyagi 980-8578, Japan

Published online: 15 October 2016

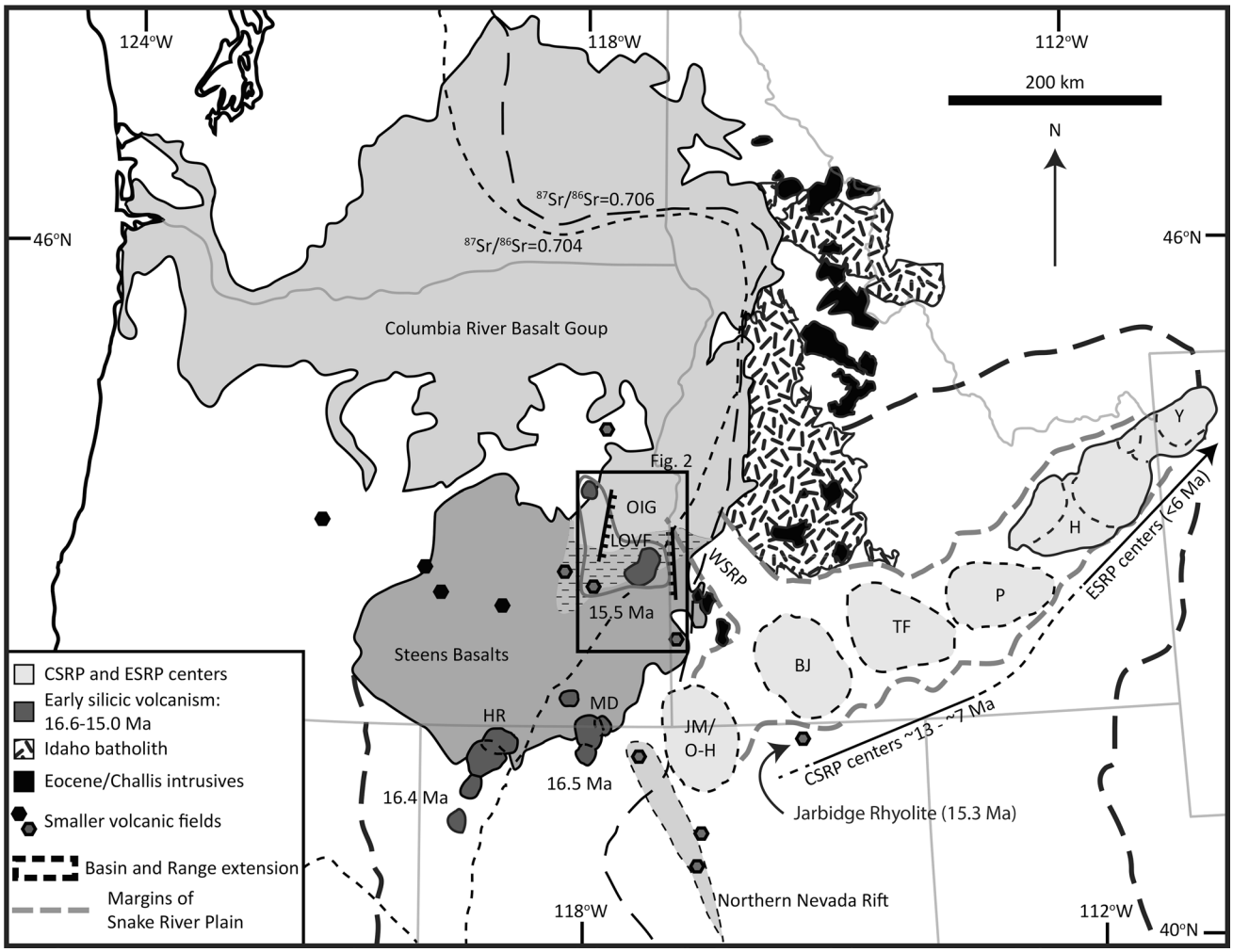


**Fig. 1** Map of mid-Miocene to present Snake River Plain–Yellowstone (SRP-Y) volcanism, as well as relevant adjacent provinces (after Coble and Mahood 2012). The $^{87}Sr/^{86}Sr = 0.704$ and $^{87}Sr/^{86}Sr = 0.706$ lines delineate the transition from accreted terranes to the west, into the cratonic lithosphere to the east. Abbreviations: *BJ* Bruneau-Jarbidge; *H* Heise; *HR* High Rocks; *JM/O–H*, Juniper Mountain/Owyhee Humboldt; *LOVF* Lake Owyhee volcanic field; *MC* McDermitt; *OIG* Oregon-Idaho Graben; *P* Picabo; *TF* Twin Falls; *WSRP* Western Snake River Plain; *Y* Yellowstone

for rhyolites at Yellowstone, greater than 10,000 $km^3$ of felsic volcanic rock derived from low-$\delta^{18}O$ magma have been identified within the SRP-Y. These low-$\delta^{18}O$ magmas offer constraints on the timing and duration of meteoric hydrothermal alteration, as well as subsequent melting and assimilation, and inform us about the construction and dynamics of magma chambers that have fed large-volume caldera-forming eruptions for the last ~16 Myr. Additionally, understanding the origin of large low-$\delta^{18}O$ magmatic provinces aids the accurate interpretation of low-$\delta^{18}O$ magmas in the geological record (e.g., Taylor 1986; Valley et al. 2005; Bindeman and Serebryakov 2011; Fu et al. 2012).

Zircon has been widely used in oxygen isotope studies, as *pristine crystalline* (i.e., not radiation damaged) zircon is both physically and chemically resistant, and possesses slow oxygen diffusion rates (Valley et al. 1994; Cherniak and Watson 2003; Bowman et al. 2011); thus, it offers a robust record of magmatic oxygen isotope compositions during crystallization. This allows oxygen isotope ratios in zircon to place constraints on petrologic processes, material mass balance within magmatic systems, and estimates of magmatic $\delta^{18}O$ values. In contrast, whole rock and/or phenocryst phases can variably reflect subsolidus alteration.

Within the SRP-Y, in situ oxygen isotope analyses of zircon by ion microprobe reveal cryptic details of magmatic and hydrothermal processes, by documenting complex $\delta^{18}O$ growth histories for single grains and magmatic trends in successive emplacement units (e.g., Bindeman et al. 2008). The number and variety of models for SRP-Y low-$\delta^{18}O$ magma genesis reflect both variability in the ubiquity and magnitude of $\delta^{18}O$(magma) lowering in SRP-Y centers, as well as general uncertainties in meteoric water

fluxes at depth (e.g., Taylor 1986), crust- versus mantle-derived magma mass balance (e.g., McCurry and Rodgers 2009; Simakin and Bindeman 2012), and the thermal constraints on the efficiency of crustal fusion and longevity of crustal magma systems (Leeman et al. 2008; Annen 2009; Gelman et al. 2013). Generating large regions of low-$\delta^{18}O$ crust, like those required based on mass balance in the SRP-Y, demands pervasive oxygen exchange between meteoric water and rocks at high temperatures. Water–rock exchange is in part controlled by the permeability, temperature, and fluid pressure regimes of the crust and large-scale meteoric hydrothermal systems. It is difficult for surface waters to circulate in large quantities to depths >10 km due to decreasing permeability and porosity, and variable fluid pressure regimes with depth (e.g., Valley 1986; Ingebritsen and Manning 2010). For large magmatic systems, this places a limit on the depth of meteoric hydrothermal alteration, and thus a limit on the depth of assimilation melting and assimilation processes in the case of low-$\delta^{18}O$ magmas. However, generating large volumes of eruptible low-$\delta^{18}O$ melt by assimilation is more difficult at shallow depths due to lower ambient wall rock temperatures and rapid dissipation of thermal energy (Leeman et al. 2008). Establishing the appropriate timing and depth of alteration relative to magma production in the SRP-Y must take into account time-dependent crustal permeability and fluid pressure conditions, as well as the thermal inputs required to drive both hydrothermal alteration and crustal assimilation. A robust model for the genesis of low-$\delta^{18}O$ magmatism within the SRP-Y revolves around explaining the *timing and distribution of hydrothermally altered material*, and its relation to hotspot magmatism.

The caldera systems of the Lake Owyhee volcanic field (LOVF) in eastern Oregon represent some of the earliest manifestations of the SRP-Y hotspot track (Coble and Mahood 2012). The detailed oxygen isotope characterization of the LOVF, and other centers west of the $^{87}Sr/^{86}Sr = 0.706$ line are critical to determining the presence and abundance of low-$\delta^{18}O$ SRP-Y magmas west of the cratonic boundary. While several studies have documented low-$\delta^{18}O$ magmas within the LOVF (Blum et al. 2012, 2013; Colon et al. 2015a), the magmatic oxygen isotope trends within the LOVF (and other early, >15 Ma, centers) remain less well characterized relative to the central and eastern segments of the SRP-Y. Published models for LOVF low-$\delta^{18}O$ magma genesis rely on relatively few samples, and thus present a limited view of $\delta^{18}O$(magma) trends as a function time and space. The robust assessment of low-$\delta^{18}O$ magma trends in the LOVF requires a more thorough sampling within the field. Additionally, extrapolating between low-$\delta^{18}O$ magma genesis within the LOVF and that of the greater SRP-Y is more effectively accomplished while considering the $\delta^{18}O$ trends within both SRP-Y centers and the surrounding regions.

This work presents in situ oxygen isotope and U–Pb analyses of zircon, as well as laser fluorination oxygen isotope analyses of phenocrysts, from throughout the LOVF. These data provide a detailed record of magmatic $\delta^{18}O$ in time and space, and expand the known volume of low-$\delta^{18}O$ magmas in the SRP-Y, particularly those west of the cratonic boundary ($^{87}Sr/^{86}Sr = 0.706$), that are constrained by in situ zircon analyses. These data, in addition to (1) compiled in situ zircon oxygen isotope data for the majority of SRP-Y centers, and (2) a compilation of regional $\delta^{18}O$(WR) and $\delta^{18}O$(magma) data, support a link between pervasive alteration, low-$\delta^{18}O$ magmatism, and hotspot-derived thermal inputs. When considered in concert with the structural and $\delta^{18}O$ evolution of SRP-Y centers, we suggest that SRP-Y low-$\delta^{18}O$ magmas are best explained by $\delta^{18}O$ lowering of the SRP-Y crust though large-scale meteoric hydrothermal circulation driven by the superposition of high, hotspot-derived (syn-hotspot) thermal fluxes on extensional tectonics. This general model has implications for the tectonic associations of other large low-$\delta^{18}O$ igneous provinces where similar thermal and structural states coincide to generate temporally associated meteoric hydrothermal alteration and subsequent assimilation, and produce low-$\delta^{18}O$ magmas.

## Regional setting and existing models for SRP-Y low-$\delta^{18}O$ magmas

The SRP-Y hotspot track extends from the currently active Yellowstone plateau volcanic field, to the southwest along the Snake River Plain, and into the Owyhee region of northern Nevada, southwestern Idaho and eastern Oregon (Fig. 1). While debate persists concerning the intricacies of a holistic geophysical model for the SRP-Y track and Steens-Columbia River Basalt Group (e.g., Fouch 2012; Darold and Humphreys 2013), age and structural trends in silicic volcanism (Pierce and Morgan 1992), seismic imaging (Obrebski et al. 2010), physical models (Kincaid et al. 2013), and geochemical tracers (Camp and Ross 2004; Camp and Hanan 2008) are consistent with time-transgressive magmatism driven by a mantle plume. During 16.6–15.0 Ma flood basalt volcanism, an estimated 4–10 $\times$ $10^3$ $km^3$ of rhyolitic volcanic rocks erupted across northern Nevada, eastern Oregon, and southwestern Idaho (Coble and Mahood 2012; Cummings et al. 2000) as part of pre—15.0 Ma bimodal SRP-Y volcanism. The centers associated with this rhyolitic volcanism, including the LOVF, are the earliest centers strongly associated with the SRP-Y hotspot. After ~15 Ma, SRP-Y volcanism crossed into cratonic lithosphere, delineated by the $^{87}Sr/^{86}Sr = 0.706$ line (Armstrong et al. 1977; Leeman et al. 1992); it has since

followed a trend younging to the northeast, opposite to the inferred motion of the North American plate (Rodgers et al. 2002). Post-15 Ma SRP-Y volcanism is generally dry and bimodal (basalt–rhyolite). Individual volcanic centers undergo several climactic eruptive cycles during 2–4 million years of activity, after which basaltic volcanism dominates (Perkins and Nash, 2002). While the vast majority of SRP-Y centers share the above general trends, differences exist with respect to system lifetimes, eruptive rates, average eruptive temperatures, and magmatic $\delta^{18}O$ values (Perkins and Nash 2002; Watts et al. 2011). Several authors have documented the coupled kinematic history of the Snake River Plain and adjacent Basin and Range (Anders et al. 1989; Pierce and Morgan 1992; Parsons et al. 1998; Rodgers et al. 2002).

The Lake Owyhee volcanic field is part of widespread silicic volcanism spatially associated with flood basalts around 17–15 Ma. The LOVF was originally defined by Rytuba et al. (1991) to include several ignimbrites, and associated smaller volume domes and flows that erupted in east-central Oregon between ~16 and 14 Ma. An estimated 1100 $km^3$ of peralkaline to metaluminous silicic lavas and tuffs erupted at that time from calderas and fissures straddling the $^{87}Sr/^{86}Sr = 0.704$ line (Fig. 1; Rytuba et al. 1991; Leeman et al. 1992; Cummings et al. 2000; Coble and Mahood 2012). A subset of LOVF vents overlap the north–south-trending Oregon-Idaho Graben (OIG) (Fig. 2), a north–south-trending region of extension active between ~15.8 and 10.5 Ma (Cummings et al. 2000; Benson and Mahood 2016).

Initial mapping by Rytuba et al. (1991) included six large-volume tuffs within the LOVF. The largest and most well studied include the intragraben Leslie Gulch Tuff, an ash-flow tuff erupted from the Mahogany Mountain caldera; the intragraben Tuff of Spring Creek, an ash-flow tuff erupted from the Three Fingers caldera; and the extragraben Dinner Creek Tuff (15.9–15.3 Ma, 200–300 $km^3$), a densely welded ash-flow tuff erupted to the north (Fig. 2). Rytuba et al. (1991) also documented several pre- and post-caldera domes and flows proximal to the mapped source calderas, including the rhyolite flows of Mahogany Mountain, McIntyre Ridge, and several other unnamed units. Recently, Benson and Mahood (2016) proposed a refinement to the LOVF stratigraphy, focusing on the volcanism associated with the Mahogany Mountain and Three Fingers Calderas. Benson and Mahood (2016) conclude that the mineralogy, petrography, stratigraphic relations, geochronology, and major and trace element chemistry are all consistent with the Tuff of Spring Creek being altered portions of the Tuff of Leslie Gulch. Field observations, as well as major element and isotope data within this study, are consistent with these conclusions (see below), and we consider the Tuff of Spring Creek to be part of the Tuff of Leslie Gulch. To clarify sampling relations, we maintain an "SC" modifier for those samples previously considered part of the Tuff of Spring Creek. Benson and Mahood (2016) further infer, based on their mapping, that the source of the single Tuff of Leslie Gulch emplacement unit (inclusive of the "Tuff of Spring Creek") is a large caldera they call the Rooster

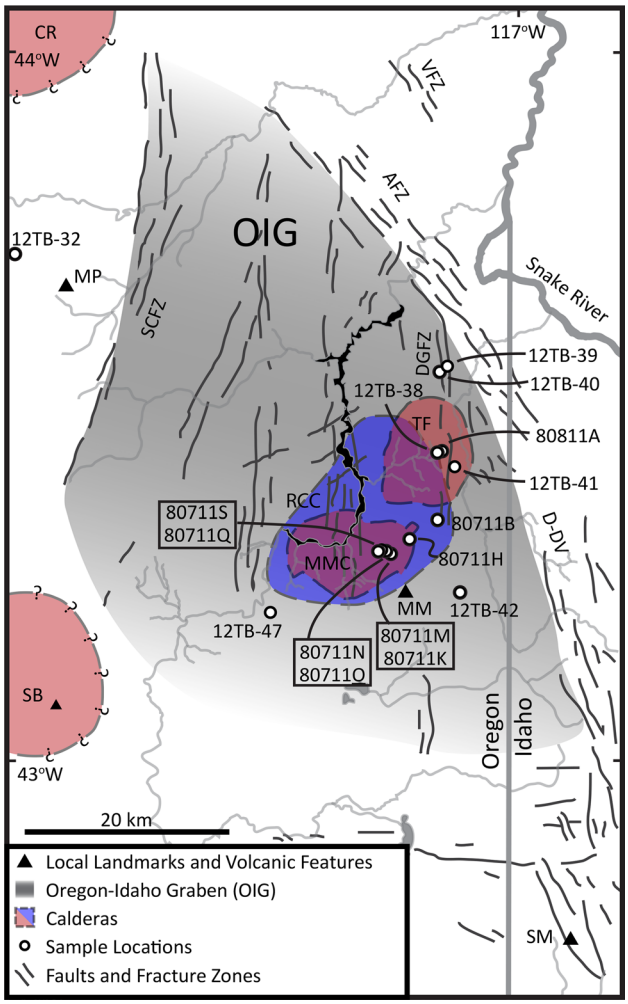


**Fig. 2** Map of the Lake Owyhee volcanic field (LOVF) including structural trends and sample locations from this study (modified from Rytuba et al. 1991; Benson and Mahood 2016). Red regions with dashed outlines demarcate caldera structures of Rytuba et al. (1991), with "?" signifying a potential, but debated, structure. The RCC is shown in blue effectively replacing the MMC and TFC as the single source of the Tuff of Leslie Gulf (inclusive of the "Tuff of Spring Creek") (Benson and Mahood 2016). The *light shaded* region indicates area of Oregon-Idaho Graben (OIG) subsidence with E–W extension along N–S-trending faults (Cummings et al. 2000). NW–SE-trending faults of the Adrian fault zone and Vale fault zone represent younger subsidence associated with extension in the Western Snake River Plain. Abbreviations: *AFZ* Adrian fault zone; *CR* Castle Rock, *MM* Mahogany Mountain; *MMC* Mahogany Mountain Caldera; *TFC* Three Fingers Caldera; *RCC* Rooster Comb Caldera; *MP* Monument Peak; *SB* Saddle Butte; *VFZ* Vale fault zone; *SCFZ* Squaw Creek fault zone; *D-DV* Delmar-Duck Valley structural trend; *OIG* Oregon-Idaho Graben

Comb Caldera (Fig. 2; Benson and Mahood 2016). This recent mapping has helped to resolve some of the pre-/post-caldera emplacement relations within the LOVF, though the age and $\delta^{18}O$ data within this paper expand on some of the proposed unit correlations and emplacement relations.

Initial subsidence of the OIG is interpreted to either coincide with, or closely predate, the eruption of the intra-graben caldera-forming tuffs, based on ponding of caldera-forming ignimbrites in north–south-trending basin structures on the eastern margin of the OIG (Cummings et al. 2000; Ferns and McClaughry 2013; Benson and Mahood 2016). Small-volume post-LOVF volcanism persisted within the graben in the form of calc-alkaline domes and flows until ~10.5 Ma (Cummings et al. 2000). The division of the region into separate basins as well as cover by younger volcanism and basin sediments has obscured many stratigraphic relations, and further resolving stratigraphic relations is beyond the scope of this paper. We instead focus on the magmatic $\delta^{18}O$ variation through time in both large and smaller volume units, and understanding how these trends relate to the thermal, structural and hydrothermal evolution of the LOVF.

## Existing models for SRP-Y low-$\delta^{18}O$ magma genesis

Variability in the ubiquity and magnitude of $^{18}O$ depletions through time and space has motivated development of several petrogenetic models for SRP-Y low-$\delta^{18}O$ magmas. These models vary in the *timing* and *thermal driving force* for meteoric hydrothermal alteration of the SRP-Y crust, and include (1) syn-hotspot alteration (i.e., fluid circulation driven by hotspot magmatism) with wholesale remelting/batch assembly of hydrothermally altered, intracaldera volcanic/subvolcanic source rock linked to caldera subsidence (Fig. 3a; Hildreth et al. 1991; Bindeman and Valley 2000, 2001; Bindeman et al. 2001, 2007, 2008; Watts et al. 2011); (2) assimilation/wholesale melting of a preexisting (i.e., pre-hotspot) hydrothermally altered low-$\delta^{18}O$ crustal source region, typically taken to be the Idaho batholith altered by Eocene epizonal plutons, or Eocene volcanics (Fig. 3b; Boroughs et al. 2005, 2012; Drew et al. 2013); (3) long-term, pre-/syn-hotspot deep (15 km) meteoric hydrothermal circulation and alteration of the middle crust with subsequent melting (Fig. 3c; Leeman et al. 2008); and (4) modification of crustal-scale permeability structure through extensional tectonics (Fig. 3d, e; Blum et al. 2012, 2013; Blum 2013; Konstantinou et al. 2013; Drew et al. 2013; Colon et al. 2015a, b). These models are reviewed briefly below.

### *Preexisting source models*

Several models for SRP-Y low-$\delta^{18}O$ magma genesis either suggest or imply the presence of large-scale preexisting low-$\delta^{18}O$ regions within the pre-hotspot SRP-Y crust. These include assimilation of hydrothermally altered material within the Idaho batholith associated with Eocene plutonism and volcanism (Fig. 3b; Boroughs et al. 2005, 2012) and hydrothermal alteration of SRP-Y crust under general crustal-scale permeability and thermal gradients (Fig. 3c; Leeman et al. 2008).

Models promoting the assimilation of hydrothermally altered material within the Idaho batholith focus on the well-documented low-$\delta^{18}O$ regions associated with Eocene magmatism/volcanism in and around the Idaho batholith (Boroughs et al. 2005, 2012; Drew et al. 2013). Given the difficulty in generating large volumes of eruptible magma, particularly at shallow depths, this model is advantageous from an energetics standpoint; the energy required to drive hydrothermal alteration of the crust and subsequent melting are divided between different magmatic episodes. The applicability of this model to the SRP-Y as a whole is debated, primarily due to (1) questions about whether the volume, $\delta^{18}O$(WR), and concentration of low-$\delta^{18}O$ rock within the Idaho batholith are sufficient to generate the low-$\delta^{18}O$ magmas of the CSRP; (2) the fact that the Eocene alteration of the Idaho batholith is only observed adjacent to the CSRP, and yet low-$\delta^{18}O$ magmas occur throughout the SRP-Y; and (3) the normal- to high-$\delta^{18}O$ character of xenoliths within the CSRP (Watts et al. 2010). These relations are further explored below using a new compilation of $\delta^{18}O$(WR) and $\delta^{18}O$(magma) data for the SRP-Y and adjacent regions to the north of the SRP-Y.

Other authors have modeled meteoric hydrothermal alteration, and the resulting $\delta^{18}O$ profile of the crust, using general, crustal-scale permeability models (Ingebritsen and Manning 1999), and a Basin and Range geothermal gradient (Leeman et al. 2008). This work evaluates the energy budget required for genesis of large volumes of magmas within the crust. While the ability of this model to capture regional, center-to-center, and unit-to-unit $\delta^{18}O$ trends is unclear, the geothermal gradient and permeability relations used within the model are general, and not restricted in time or space to the SRP-Y. This model hypothesizes the presence of a stratified and laterally continuous region of low-$\delta^{18}O$ crust both within and outside of the SRP-Y. In fact, the assumptions supporting this model would apply to many terranes *globally*; yet, evidence for such a $\delta^{18}O$ stratification of the continental crust is lacking. Below we look at the spatial nature of $\delta^{18}O$(WR) trends within the Basin and Range in order to examine whether there is evidence that the tectonic evolution of the western USA has resulted in widespread low-$\delta^{18}O$ stratification of the crust.

### *Caldera subsidence models*

In this class of models, low-$\delta^{18}O$ magmas form in response to caldera-forming eruptions, as low-$\delta^{18}O$ rocks within the

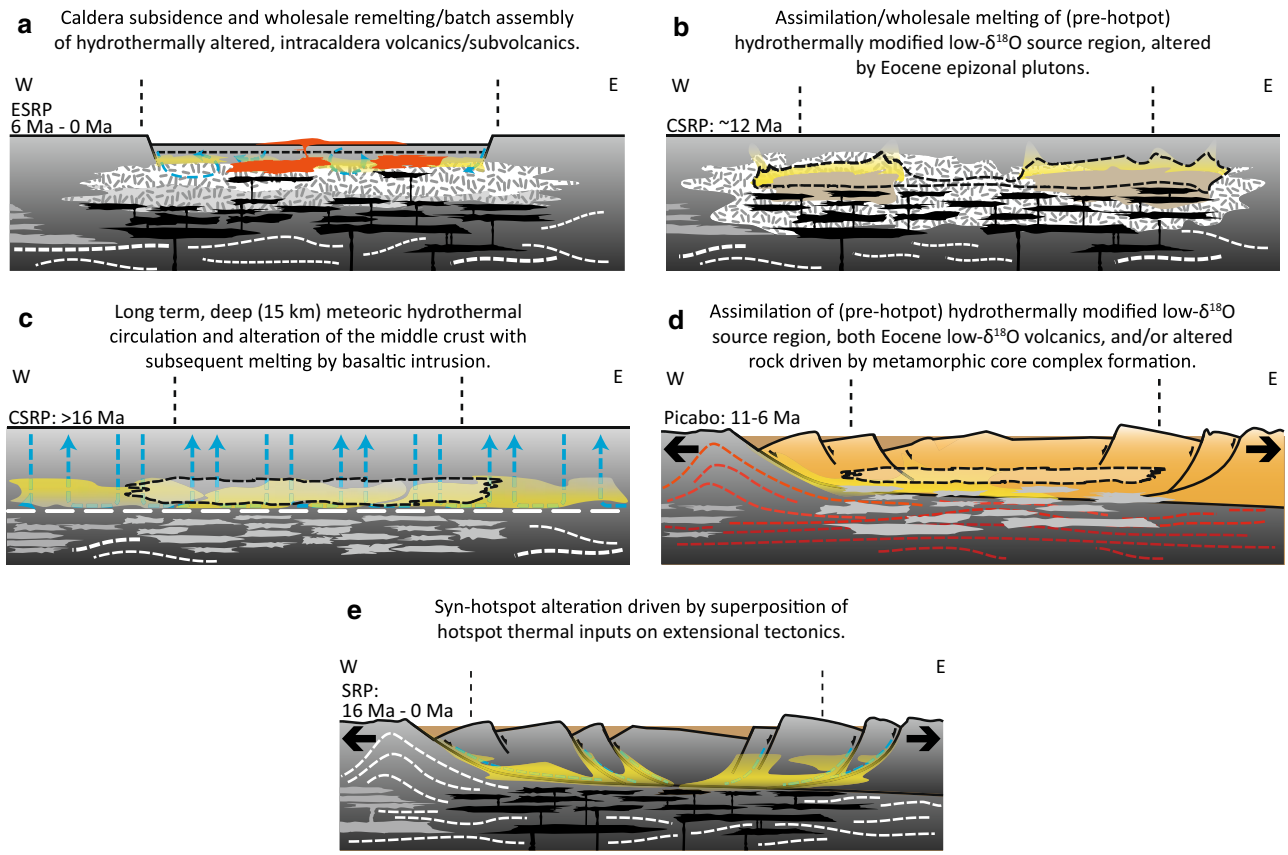


**Fig. 3** Schematic representations of models for SRP-Y low-$\delta^{18}O$ magma genesis at caldera-scale, emphasizing relevant structural, thermal, and geological associations within the mid- to upper crust. Blue dashed lines represent generalized meteoric water flow paths, and yellow regions represent areas of low-$\delta^{18}O$ crust, with black dashed outlines delineating the regions of crustal melting. Each cross section is oriented east–west, parallel to the axis of the Snake River Plain-Yellowstone hotspot track, with vertical dashed lines delineating the approximate locus of active magmatism at the time indicated for each diagram. The time and location for which the proposed model is applicable, and the "type locality" for that model, are to the upper left of each cross section. Basalts are shown in black. See text for further discussion. **a** Caldera subsidence model, (Hildreth et al. 1991; Bindeman and Valley 2000, 2001; Bindeman et al. 2008; Watts et al. 2011). Hatched patterns are plutonic equivalents to successive caldera-forming eruptions. **b** Pre-hotspot low-$\delta^{18}O$ source model, with assimilation and melting of hydrothermally altered low-$\delta^{18}O$ Idaho batholith (white, hatched). Alteration driven by Eocene epizonal intrusions (tan) (Boroughs et al. 2005, 2012). **c** Long-term, deep (~15 km) meteoric hydrothermal circulation and alteration. Gray sills represent the location of future basaltic intrusions during hotspot magmatism (Leeman et al. 2008). **d** Pre-hotspot alteration through assimilation and melting of Eocene low-$\delta^{18}O$ volcanic rocks, as well as hydrothermal alteration driven by core complex formation (Konstantinou et al. 2013; Drew et al. 2013). **e** Superposition of hotspot-derived thermal fluxes on extensional tectonics (Blum et al. 2012, 2013; Drew et al. 2013; Colon et al. 2015a, b)

crustal section (formed by earlier magmas of the same volcanic center driving hydrothermal alteration) are displaced downward, and undergo bulk-remelting/assimilation during subsequent magmatism (Fig. 3a; Hildreth et al. 1991; Bindeman and Valley 2000, 2001; Bindeman et al. 2008; Watts et al. 2011). The downward displacement of low-$\delta^{18}O$ material and its subsequent melting/assimilation can be associated either with a single caldera cycle (Bindeman et al. 2008), or with several caldera cycles (Watts et al. 2011). This general model has been successful within some centers in explaining the $\delta^{18}O$ zoning trends in zircon, as well as the decrease in $\delta^{18}O$ for rhyolites erupted following caldera subsidence. In the Heise and Yellowstone centers, low-$\delta^{18}O$ volcanism is primarily (though not exclusively) restricted too post-climatic, intracaldera volcanism (Hildreth et al. 1991; Bindeman and Valley 2000; Bindeman et al. 2008) or late-stage ignimbrites (Watts et al. 2011). Paired oxygen and U–Pb ion microprobe analyses in zircon document concomitant inheritance from earlier caldera cycles and low-$\delta^{18}O$ magmatism (Bindeman et al. 2007, 2008; Watts et al. 2011). These data have been taken to link the genesis of low-$\delta^{18}O$ magmas with the downward displacement of hydrothermally altered rocks during caldera subsidence, and imply that low-$\delta^{18}O$ magmas form in

response to (but not prior to) caldera subsidence within a given center.

While this model is successful in describing the low-$\delta^{18}O$ magmas of the Yellowstone, Heise and, to a lesser extent, Picabo centers, several authors have noted the difficulty in applying a caldera subsidence model for the genesis of low-$\delta^{18}O$ magmas in the greater SRP-Y, and particularly the centers of the CSRP (Boroughs et al. 2005, 2012). Foremost, there exist no, or very few, normal-$\delta^{18}O$ magmas within the CSRP (Cathey et al. 2008; Seligman 2012), which is problematic given this model dictates large-volume normal-$\delta^{18}O$ caldera-forming eruptions to occur prior to the onset of low-$\delta^{18}O$ magmatism. In addition, caldera structures as well as caldera-forming/post-caldera stratigraphic relations are obscured within the CSRP, making variability from unit-to-unit difficult to link directly to caldera subsidence processes. In expanding the $\delta^{18}O$ record for SRP-Y centers that is constrained by zircons, the present study of LOVF magmatism offers further insight as to the importance of caldera subsidence to the low-$\delta^{18}O$ magmatism of the greater SRP-Y.

*Models involving extensional tectonics*

It has been suggested that extensional tectonics may play a critical role in the development of low-$\delta^{18}O$ magmas. Such models focus on the modified crustal-scale permeability structure induced by brittle fracture and faulting within the crust, and the displacement of material downward within the crustal column to where melting and assimilation are more energetically favorable (Taylor 1986; Blum et al. 2012, 2013; Blum 2013; Drew et al. 2013; Colon et al. 2015a, b). These models capture aspects of the crustal-scale permeability structure which are unique to the Basin and Range and SRP-Y crust. There remain subtle, yet significant, differences in these models given they differ primarily in the *timing and thermal driving source for meteoric hydrothermal alteration*. These models include both pre-/syn-hotpot hydrothermal alterations, driven by metamorphic core complex formation (Fig. 3d; Konstantinou et al. 2013; Drew et al. 2013), as well as syn-hotspot alteration driven by hotpot-derived thermal inputs to the crust (Fig. 3e; Blum et al. 2012, 2013; Blum 2013; Drew et al. 2013; Colon et al. 2015a, b). The structural and thermal associations within these models have implications for the presence of low-$\delta^{18}O$ source regions both within and outside the SRP-Y. The synthesis of $\delta^{18}O$(WR) data for silicic volcanic rocks and basement lithologies from throughout the Basin and Range (below) allows evaluation of the regional uniqueness of the SRP-Y (with respect to $\delta^{18}O$) and discerning the thermal and structural relationships which may control the timing and extent of alteration.

## Samples and methods

Lake Owyhee volcanic field samples come from the large-volume caldera-forming tuffs, the Dinner Creek Tuff and the Tuff of Leslie Gulch, as well as several smaller volume pre- and post-caldera silicic units (Fig. 2). Sample location information, inferred emplacement relations, and mapping references for LOVF samples are summarized in Table 1 and Fig. 4a. Samples underwent standard crushing, sieving, and density separation procedures to isolate phenocrysts for laser fluorination analyses, as well as zircons for grain-scale imaging and oxygen isotope analysis by ion microprobe. Hand-picked quartz and K-feldspar were analyzed by multi-grain laser fluorination analyses following the procedures of Valley et al. (1995). Gore Mountain garnet standard (UWG-2, $\delta^{18}O = 5.80 \pm 0.1$ ‰ (2SD), SMOW, Valley et al. 1995) was analyzed to correct for small day-to-day variations in analysis conditions, with a maximum daily correction of 0.06 ‰. Sample sizes ranged between 1.07 and 2.56 mg, and uncertainty for all but the smallest sample analysis was ±0.2 ‰ (2 S.D.), based on replicate analyses of UWG-2.

Following separation, individual zircon grains were cast in epoxy, ground to approximately half depth, polished to <1 micron relief, and characterized by secondary electron, backscattered electron, and cathodoluminescence imaging by scanning electron microscope (SEM). Imaging reveals a variety of internal textures including oscillatory and sector zoning (both typical of magmatic zircon), as well as curvilinear internal boundaries which are interpreted as episodes of dissolution (Online Resource 1). Uncommon anhedral, non-cathodoluminescent zircons are also observed within a subset of LOVF units.

Zircon oxygen isotope analyses by ion microprobe were made at the WiscSIMS Laboratory, UW-Madison during three separate sessions following the procedures of Kita et al. (2009) using a 10–15 μm spot with KIM-5 zircon as the oxygen isotope standard ($\delta^{18}O = 5.09 \pm 0.09$ ‰ SMOW; Valley, 2003). The majority of analyzed LOVF zircons were targeted in both core and rim domains, as identified by cathodoluminescence imaging, to evaluate the presence/absence of oxygen isotope zonation. Analysis pits were imaged by SEM, and compromised analyses (identified by the presence of inclusions and/or pit irregularities) are excluded from consideration in the following discussion. In those instances where we are interested in relating $\delta^{18}O$(Zrc) to $\delta^{18}O$(magma), we have used measured whole-rock chemistry (see below), and the empirical relationship of Lackey et al. (2008):

$$\Delta^{18}O(WR - Zrc) \approx 0.0612(\text{wt.\% } SiO_2) - 2.50‰$$

After SIMS oxygen isotope analyses, grains were ground and polished to remove SIMS pits, and laser

**Table 1** Summary of location information and inferred emplacement relations for samples in this study from the Lake Owyhee volcanic field

| Sample | Unit | Location | | Emplacement/sample type | Ref.[†] |
|---|---|---|---|---|---|
| | | Latitude | Longitude | | |
| 12TB-32 | Dinner Creek Tuff (DCT) | 43.705° | −117.9948° | Outflow facies of DCT | 1, 2 |
| 12TB-42 | Mahogany Mountain rhyolite (MMr) | 43.2381° | −117.1209° | Post-TLG | 3, 4 (pre) 5, 6 (post) |
| 80711H | Tuff of Leslie Gulch (TLG1) | 43.3144° | −117.2177° | TLG ash-fall | 3, 4, 6, 7 |
| 80711Q | Tuff of Leslie Gulch (TLG2) | 43.2996° | −117.2704° | TLG ash-fall | 3, 4, 6, 8 |
| 80711N | Tuff of Leslie Gulch-SC (TLG-SC1) | 43.2965° | −117.2586° | TLG-SC caldera fill | 4, 6, 8 |
| 80711Q | Tuff of Leslie Gulch-SC (TLG-SC2) | 43.2967° | −117.2584° | TLG-SC caldera fill | 4, 6, 8 |
| 80711M | Rhyolite dike (Rd1) | 43.2946° | −117.2542° | Resurgent intracaldera dike, post-TLG | 4, 6, 8 |
| 80711K | Rhyolite dike (Rd2) | 43.2943° | −117.2530° | Resurgent intracaldera dike, post-TLG | 4, 6, 8 |
| 80711S | Rhyolite dike (Rd3) | 43.2979° | −117.2772° | Resurgent intracaldera dike, post-TLG | 4, 6, 8 |
| 80711B | Bannock Ridge rhyolite (BRr) | 43.3410° | −117.1639° | Post-TLG | 3, 6, 7 |
| 12TB-40 | Devil's Gate rhyolite (DGr) | 43.5471° | −117.1621° | Post-TLG-SC | 6, 9, 10 |
| 80811A | Rhyolite of Mcintyre Ridge (MRr1) | 43.4373° | −117.1561° | Pre-TLG-SC (dome/flow) | 3, 6 (pre), 11 (post) |
| 12TB-38 | Rhyolite of Mcintyre Ridge (MRr2) | 43.4334° | −117.1653° | Pre-TLG-SC (dome/flow) | 3, 6 (pre), 11 (post) |
| 12TB-41 | Round Mountain (rhyolite porphyry) (RMr) | 43.4137° | −117.1373° | Post-TLG-SC (dome/flow) | 3, 6, 11 |
| 12TB-39 | Sanidine rhyolite (Sr) | 43.5541° | −117.1525° | Post-TLG-SC (dome/flow) | 3, 9 |
| 12TB-47 | Birch Creek Tuff (BCT) | 43.2062° | −117.4937° | BCT | 3, 6 |

[†] References: 1. Ferns et al. (1993a); 2. Evans (1996); 3. Ferns et al. (1993b); 4. Vander Meulen (1989); 5. Macleod (1989); 6. Benson and Mahood (2016); 7. Vander Meulen et al. (1987a); 8. Vander Meulen et al. (1987b); 9. Ferns (1988); 10. Cummings et al. (2000); 11. Vander Meulen et al. (1989)

ablation–inductively coupled plasma–mass spectrometry (LA-ICP-MS) U–Pb dating was undertaken to expand the data set of ages for LOVF units, as well as to look for evidence of inheritance in LOVF zircon cores. Measurements were completed at the University of Arizona LaserChron Laboratory using a Nu Plasma HR MC-ICP-MS. Analyses used a 30–35 μm spot size (pits are ~10–12 μm deep), with internal laboratory zircon standards Sri Lanka zircon (563.5 ± 2.3 Ma; Gehrels et al. 2008) and R33 (419.3 ± 0.4 Ma; Black et al. 2004) run as primary and secondary standards, respectively. Raw data were processed in laboratory following the procedures of Gehrels et al. (2008), followed by further processing in Isoplot 3.75 (Ludwig 2012). Further analytical details can be found in Online Resource 3. U–Pb analyses targeted domains proximal to oxygen isotope analyses. The larger spot size (~ 35 μm) for U–Pb dating and the desire to avoid inclusions did not allow direct correlation of spots in certain cases. Due to young ages, relatively low uranium concentrations, and the rapid emplacement of LOVF units, the analytical precision for U–Pb data is sufficient to identify xenocrystic zircons, but not to resolve detailed emplacement relations.

Whole-rock geochemical data were collected for all the samples for which zircon oxygen isotope data were collected. Whole-rock powders (15–25 g splits of crushed rock) were analyzed by X-ray fluorescence (XRF) at Washington State University following the procedure of Johnson et al. (1999). Whole-rock major and trace element data are included in Online Resource 5.

## Results

### U–Pb zircon dating

A total of 363 U–Pb analyses were completed on LOVF zircons. For the vast majority, young ages and relatively low U and Th contents act as a limit for the achievable precision (see Online Resource 4). Analyses with uncertainties >30 % were excluded from consideration. Based on this criterion, 291 out of 363 total analyses were considered to have acceptable precision to be included during data analysis, with $^{206}Pb/^{238}U$ ages between 12.4 and 20.9 Ma, and uncertainties between 1.7 and 29.6 %.

In all cases, individual $^{206}Pb/^{238}U$ ages from spot analyses overlap the weighted mean ages for individual units at 2SD. While textural evidence exists for complex zircon growth histories (see Online Resource 1), the uncertainty for individual age analyses cannot resolve the complexities of the zircon crystallization histories. As a result, the weighted mean ages for each sample are taken as the best estimate of eruption/emplacement age, at least in cases where higher resolution age constraints do not already exist. Weighted mean $^{206}Pb/^{238}U$ ages within this study constrain LOVF magmatism between 15.4 ± 0.79 Ma and

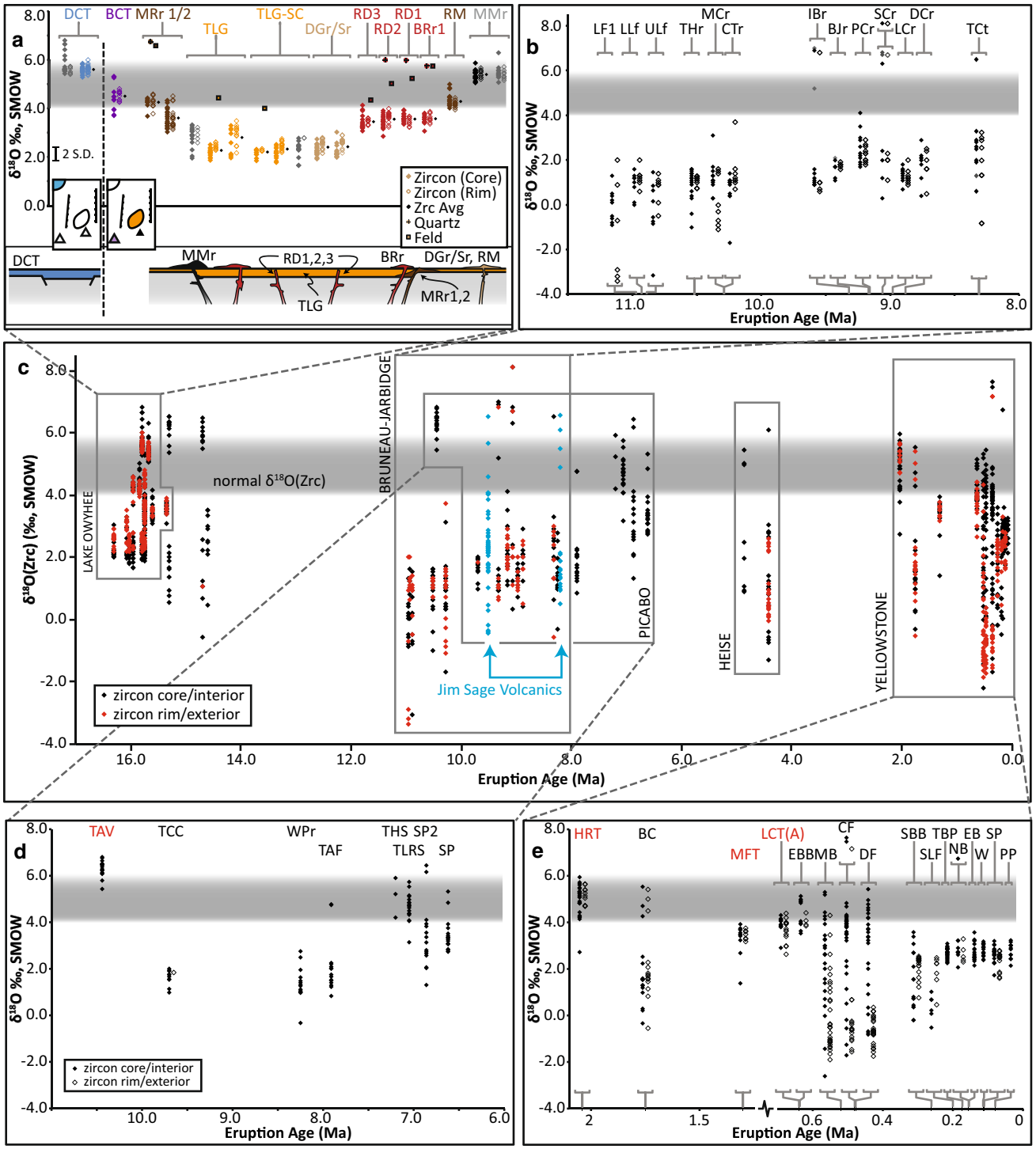


**Fig. 4** Oxygen isotope data for SRP-Y rhyolites. **a** $\delta^{18}O$(Zrc) (by SIMS) and other phenocrysts (by laser fluorination) from LOVF rhyolites (16.3-15.4 Ma). Sample location and reference information are in Table 1. Data are summarized in Table 2 and Online Resource 2. Gray data points are zircon data from Colon et al. 2015a. Small insets show generalized source regions within the LOVF (correlate with Fig. 2). Schematic emplacement relations are shown along bottom. No detailed time relation is implied on the abscissa outside of general pre-/post-caldera relations within each source region. See Table 1 for LOVF unit abbreviations. **b** Bruneau-Jarbidge eruptive center plotted versus eruptive age. **c** Compilation of SIMS $\delta^{18}O$(Zrc) analyses versus eruptive age for the entire Snake River Plain–Yellowstone terrane. **d** Picabo eruptive center, plotted versus eruptive age. **e** Yellowstone eruptive center plotted versus eruption age. Caldera-forming eruptions for **d** and **e** are shown in *red*. (Data from Bindeman et al. 2008; Watts et al. 2011; Seligman 2012; Drew et al. 2013; Watts et al. 2012; Konstantinou et al. 2013; Wotzlaw et al. 2014; Colon et al. 2015a; this study)

16.3 ± 0.48 Ma (Table 2; Online Resources 3 and 4), and all 16 samples have weighted mean $^{206}Pb/^{238}U$ ages that are indistinguishable at the 95 % confidence level. These ages are largely indistinguishable from published data, including the Tuff of Leslie Gulch and Dinner Creek Tuff, though some notable exceptions occur for smaller units (Table 2). In the case of the Tuff of Leslie Gulch, all zircon analyses from the four separate samples give an age of 15.97 ± 0.29 Ma (2 S.D.), which is in good agreement with the 15.81 ± 0.05 Ma age measured by Benson and Mahood (2016) by Ar–Ar. The zircon U–Pb data here link the volcanism of Round Mountain (sample 12TB-41) and Bannock Ridge (80711B) to the time of LOVF volcanism, though both units have previously been interpreted as younger. In the context of constraining low-$\delta^{18}O$ magma genesis within the LOVF, our U–Pb data set serves to (1) further constrain the window of LOVF magmatism to between 16.3–15.4 Ma, and (2) demonstrate no evidence for xenocrystic zircon within the LOVF.

## Oxygen isotopes

A total of 491 in situ zircon analyses on 288 grains originating from 17 LOVF samples and 9 LOVF silicic units have a total range in $\delta^{18}O$(Zrc) from 1.8 to 6.0 ‰ SMOW (Table 1, 2; Online Resource 2). Despite this >4.0 ‰ range, zircons from individual 2–5 kg samples exhibit more limited intergrain and intragrain variability (Figs. 4a, 5a). Of the analyzed zircon domains (i.e., individual zircon cores and rims), 67 % (329 out of 491 $\delta^{18}O$ analyses) represent unambiguous growth in low-$\delta^{18}O$ magmas (i.e., $\delta^{18}O$(Zrc) <4.0 ‰). Within a single-hand sample, the 2 S.D. of zircon analyses range from 0.27 ‰ to 0.96 ‰, with $\delta^{18}O$(Zrc-max) – $\delta^{18}O$(Zrc-min) <1.7 ‰ (Table 2). Only 37 of the 201 total core–rim pairs (~ 18 %) demonstrate analytically significant core–rim oxygen isotope zoning at the 95 % confidence level (Fig. 5a; Online Resource 1 and 2). A subset of analyses targeted grain domains that are texturally ambiguous (dark, anhedral, etc.), and these analyses show no statistically significant difference in $\delta^{18}O$ from those analyses in texturally pristine domains. While the majority of zircons have homogeneous $\delta^{18}O$ with limited intergrain variability, statistically significant $\delta^{18}O$ zonation and textural growth discontinuities are consistent with a subset of zircons being zoned in $\delta^{18}O$ due to complex growth histories in magma batches with variable $\delta^{18}O$ or temperature. In other zircons, spot analyses are able to resolve textural domains *spatially*, though there is no analytical evidence or heterogeneity; thus, despite relatively homogeneous $\delta^{18}O$ for the majority of samples, we do not assume all zircon growth domains within the samples correlate directly to the erupted magma, but instead relate to growth within discrete magma batches in the LOVF system.

Multi-crystal quartz and feldspar analyses by laser fluorination were completed for a subset of samples in which zircons were analyzed. These analyses give quartz $\delta^{18}O$ values between 5.7 ‰ and 6.8 ‰, and feldspar values between 4.0 ‰ and 6.6 ‰ (Table 2). When compared with individual zircon analyses, $\Delta^{18}O$(Qtz-Zrc) fractionations range from 1.9 to 3.2 ‰, and $\Delta^{18}O$(Kfs-Zrc) fractionations are smaller and more variable at −0.16 ‰ to 2.8 ‰. Given the anticipated quartz–zircon and feldspar–zircon fractionations at magmatic temperatures ($\Delta^{18}O$(Qtz-Zrc) = 1.7–2.3 ‰, and $\Delta^{18}O$(Kfs-Zrc) = 1.1–1.5 ‰ at 800–970 °C; Clayton et al. 1989; Valley et al. 2003), a subset of the quartz–zircon and feldspar–zircon data are not in high-temperature equilibrium. Disequilibrium fractionations may exist due to inheritance of phases within the pre-eruptive magma system, subsolidus alteration of less resistant phases, averaging of distinct growth domains within laser analyses, or any combination of the above. The ranges and systematic trends in $\delta^{18}O$(Zrc) are thus the focus of the following discussion.

Several relations within the $\delta^{18}O$(Zrc) data help to resolve aspects of LOVF stratigraphy. First, the consistency in $\delta^{18}O$(Zrc) values for the Tuff of Leslie Gulch and Tuff of Spring Creek (TLG-SC), both in this study and from Colon et al. (2015a), is consistent with the interpretations of Benson and Mahood (2016): that the Tuff of Spring Creek is a variably altered portion of the Tuff of Leslie Gulch. High loss-on-ignition and major element data from TLG-SC samples within this study are also consistent with the data and conclusions of Benson and Mahood (2016) (see Online Resource 5). Secondly, the geochronology and field relations of Benson and Mahood (2016) support the interpretation that both the lower Mahogany Mountain rhyolites and Bannock Ridge rhyolites are post-caldera (see references in Table 1); however, the $\delta^{18}O$(Zrc) data for these two units are distinct and suggest that these units represent distinct emplacement units.

This study significantly expands the $\delta^{18}O$ sampling within the LOVF. The data presented here are consistent with those of Colon et al. (2015a) (see Fig. 4), who presented data for the Tuff of Leslie Gulch (and "Tuff of Spring Creek"), Dinner Creek Tuff, and Mahogany Mountain rhyolite. The broad sampling of LOVF units (this study) documents that all the sampled intragraben LOVF units, with the exception of the Mahogany Mountain rhyolite ($\delta^{18}O$(Zrc) = 5.39 ± 0.37 ‰), possess at least a subset of low-$\delta^{18}O$(Zrc) analyses, and thus contain zircons grown in low-$\delta^{18}O$ magmas (Fig. 4). We further note that low-$\delta^{18}O$(Zrc) values are restricted to within the OIG, and include the caldera-forming Tuff of Leslie Gulch (inclusive of the Tuff of Spring Creek), which has the lowest $\delta^{18}O$ of all measured units, with $\delta^{18}O$(Zrc) = 2.39 ± 0.72 ‰. We also note that the large-volume *extragraben* DCT is much higher in $\delta^{18}O$ ($\delta^{18}O$(Zrc) = 5.60 ± 0.28 ‰). The

**Table 2** Summary of age and oxygen isotope data for the studied LOVF units

| Sample | Unit | Published ages | | | $^{206}Pb/^{238}U$ age | | | | $\delta^{18}O$(Zrc) | | | | $\delta^{18}O$(Qtz) | $\delta^{18}O$(Feld) |
|---|---|---|---|---|---|---|---|---|---|---|---|---|---|---|
| | | Age (Ma) | ±2SD | Ref. | Age | ±2SD | MSWD | *n* | $\delta^{18}O$(avg) | ±2SD | Max–Min | C–R Zoning | | |
| 12TB-32 | Dinner Creek Tuff | 15.3 | | 1, 2 | 15.8 | 1.1 | 0.095 | 20 | 5.60 | 0.28 | 0.71 | n | – | – |
| 12TB-42 | Mahogany Mountain rhyolite | 15.63 | 0.05 | 3 | 15.67 | 0.33 | 0.12 | 15 | 5.39 | 0.37 | 0.81 | n | – | – |
| 80711H | Tuff of Leslie Gulch | 15.81 | 0.05 | 4, 5, 6 | 15.76 | 0.55 | 0.28 | 18 | 2.26 | 0.40 | 0.75 | y(1) | – | – |
| 80711Q | Tuff of Leslie Gulch | 15.81 | 0.05 | 4, 7, 6 | 16.08 | 0.61 | 0.23 | 14 | 2.80 | 0.96 | 1.52 | y(1) | – | 4.43 |
| | *Tuff of Leslie Gulch* | | | | 15.9 | 0.39 | 0.27 | 32 | 2.50 | 0.88 | 1.62 | y(2) | | |
| 80711N | Tuff of Leslie Gulch-SC | 15.81 | 0.05 | 7, 6 | 15.96 | 0.8 | 0.04 | 11 | 2.20 | 0.27 | 0.49 | y(1) | – | 4.00 |
| 80711Q | Tuff of Leslie Gulch-SC | 15.81 | 0.05 | 7, 6 | 16.02 | 0.35 | 0.12 | 28 | 2.32 | 0.48 | 0.97 | y(5) | – | – |
| | *Tuff of Leslie Gulch-SC* | | | | 16.01 | 0.29 | 0.097 | 39 | 2.28 | 0.43 | 0.97 | y(6) | – | – |
| | **Tuff of Leslie Gulch (all)** | | | | **15.97** | **0.29** | **0.18** | **71** | **2.39** | **0.72** | **1.71** | **y(8)** | | |
| 80711M | Rhyolite dike | 14.9-14.0 | | 7, 6 | 15.74 | 1.01 | 0.12 | 14 | 3.45 | 0.48 | 1.06 | y(4) | – | 4.34 |
| 80711K | Rhyolite dike | 14.9-14.0 | | 7, 6 | 15.6 | 0.9 | 0.062 | 13 | 3.55 | 0.49 | 1.14 | y(2) | 5.97 | 5.02 |
| 80711S | Rhyolite dike | 14.9-14.0 | | 7, 6 | 15.76 | 0.66 | 0.13 | 24 | 3.56 | 0.37 | 0.72 | y(1) | 5.96 | – |
| 80711B | Bannock Ridge rhyolite | 12.7 | | 4, 5 | 15.35 | 0.79 | 0.115 | 22 | 3.57 | 0.37 | 0.81 | n | 5.72 | 5.74 |
| 12TB-40 | Devil's Gate rhyolite | 14.9-14.0 | | 8, 9 | 15.8 | 1.0 | 0.17 | 4 | 2.40 | 0.49 | 0.87 | y(6) | – | – |
| 80811A | Rhyolite of Mcintyre Ridge | 15.91 | 0.27 | 3 | 15.76 | 0.6 | 0.2 | 25 | 4.25 | 0.45 | 0.91 | y(1) | 6.75, 6.81 | 6.58 |
| 12TB-38 | Rhyolite of McIntyre Ridge | 15.91 | 0.27 | 3 | 15.96 | 0.56 | 0.16 | 13 | 3.60 | 0.76 | 1.48 | y(2) | – | – |
| 12TB-41 | Round Mountain | 14.7 | | 4, 10 | 15.85 | 0.41 | 0.23 | 32 | 4.28 | 0.47 | 1.05 | y(2) | – | – |
| 12TB-39 | Sanidine rhyolite | 14.7 | | 4, 8 | 16.31 | 0.48 | 0.14 | 19 | 2.42 | 0.60 | 1.04 | y(5) | – | – |
| 12TB-47 | Birch Creek Tuff | 16.77 | 1.09 | 3 | 15.74 | 0.57 | 0.095 | 18 | 4.50 | 0.84 | 1.61 | y(3) | – | – |
| Max | | | | | 16.31 | | | | 5.60 | | 1.48 | | | |
| Min | | | | | 15.35 | | | | 2.20 | | 0.49 | | | |

† References: 1. Ferns et al. 1993b; 2. Evans 1996; 3. Benson and Mahood 2016; 4. Ferns et al. 1993a; 5. Vander Meulen et al. 1987a; 6. Vander Meulen 1989; 7. Vander Meulen et al. 1987b; 8. Ferns 1988; 9. Cummings et al. 2000; 10. Vander Meulen et al. 1989

* Errors are external errors (include both internal and systematic uncertainties). See ESM for imaging, individual spot data, and internal and systematic uncertainties

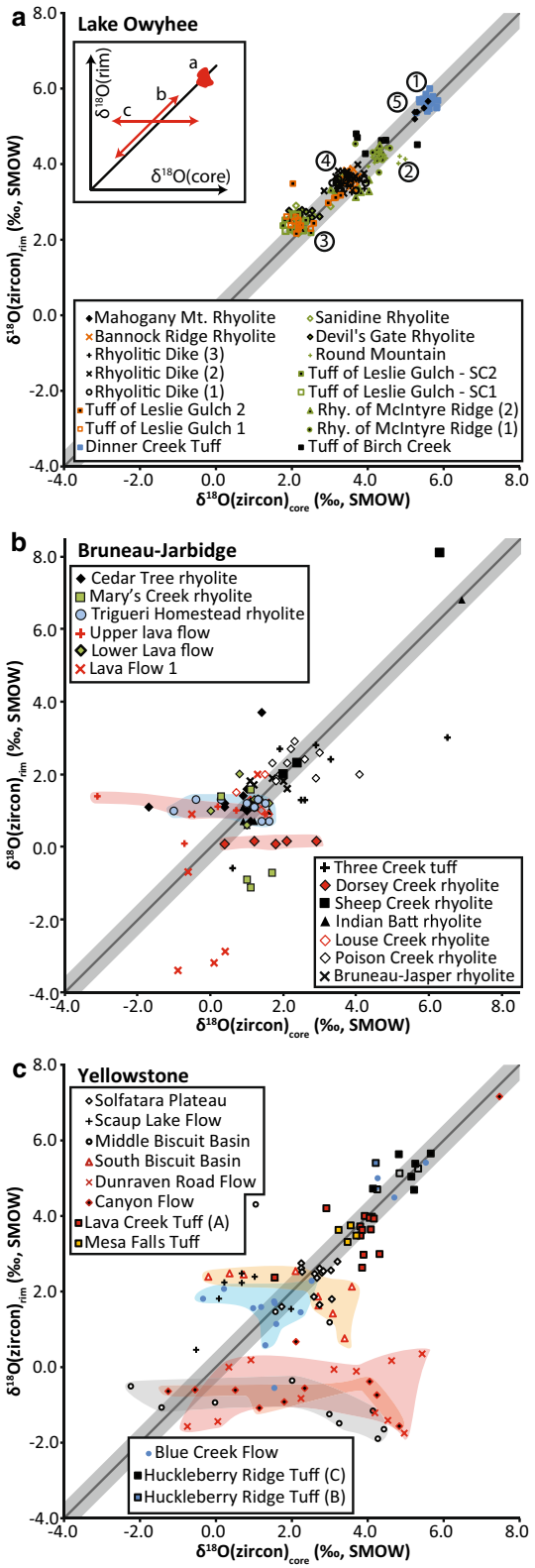


**Fig. 5** Paired $\delta^{18}O$(Zrc) core and rim analyses for zircon from SRP-Y: **a** the Lake Owyhee volcanic field (this study), **b** Bruneau-Jarbidge eruptive center (Seligman 2012), and **c** the Yellowstone caldera complex (Bindeman et al. 2008). *Solid line* represents $\Delta^{18}O$(core–rim) = 0 ‰, with dashed lines showing ±0.42 ‰ for reference. *Inset* in **a** shows trends anticipated for *a* homogeneous crystal and equilibrium core–rim relations, *b* inheritance of unzoned zircons and no rim growth in host magma, and *c* inheritance of heterogeneous zircons and rim growth from host melt. For Yellowstone and Bruneau-Jarbidge, zircons with multiple analyses in the core or rim domains (Bindeman et al. 2008) correspond to grain core and rim domains which represent the maximum $\delta^{18}O$ zoning

spatial and temporal relations within these data significantly increase the known (and zircon constrained) low-$\delta^{18}O$ magmas within both the LOVF and the greater SRP-Y, and allow for a critical review of low-$\delta^{18}O$ magma genesis in the LOVF.

## Discussion

### "Defining" low-$\delta^{18}O$ magmas

The high spatial resolution of SIMS-based oxygen isotope analyses, and the robust retention of primary chemistries and complex growth histories for many zircons, present an opportunity to probe crystallization environments which may be highly temporally or spatially localized within magma systems and/or entirely unrepresented elsewhere in the volcanic record. In the SRP-Y, we are primarily interested in resolving the patterns of low-$\delta^{18}O$ *magmatism* in time and space, and thus are concerned with identification of zircons that have crystallized from magmas with low $\delta^{18}O$ values relative to those derived from primitive sources. In order to draw general conclusions from the data regarding the presence and distribution of low-$\delta^{18}O$ magmas in the SRP-Y, we use a conservative definition of $\delta^{18}O$(Zrc) <4.0 ‰ as cutoff for what constitutes unambiguous low-$\delta^{18}O$(Zrc) values. We also note that using a value of <4.0 ‰ rather than the typical "normal-$\delta^{18}O$(Zrc)" of 5.3 ± 0.6 ‰ (2SD) only decreases the percentage of measurements in the low-$\delta^{18}O$ versus normal-$\delta^{18}O$ field for each individual eruptive center. This value is meant to distinguish between those zircons preserving unambiguous low-$\delta^{18}O$ magmas and those that retain $\delta^{18}O$ values which fall within the normal- or high-$\delta^{18}O$ range.

### Age and $\delta^{18}O$ of LOVF silicic volcanism

While age and $\delta^{18}O$(Zrc) data exist for select large-volume tuffs within the LOVF (Blum et al. 2013; Blum 2013; Colon et al. 2015a, b), the large U–Pb and oxygen isotope data set presented here represents the first in-depth and systematic study of age and $\delta^{18}O$ in the LOVF. In addition to constraining emplacement relations, these data allow for a first-order assessment of the timing, magnitude, and extent of low-$\delta^{18}O$ magmatism. We view the

comprehensive synthesis of the spatial and temporal $\delta^{18}O$ trends as a prerequisite for any robust assignment of a particular petrogenetic model for low-$\delta^{18}O$ magmas in the LOVF.

The new zircon ages measured by LA-ICP-MS further constrain LOVF low-$\delta^{18}O$ magmatism to between 16.3 and 15.4 Ma. This range is consistent with published ages and further links the LOVF temporally to the early stages of SRP-Y hotspot magmatism. The age and $\delta^{18}O$ of LOVF magmas demonstrate the growth of zircons in both high- and low-$\delta^{18}O$ magmas, but that the majority of intragraben LOVF volcanism has incorporated varying amounts of low-$\delta^{18}O$ material. The Tuff of Leslie Gulch has the lowest $\delta^{18}O$(magma) in the LOVF ($\delta^{18}O$(Zrc) = 1.8–3.5 ‰; $\delta^{18}O$(magma) = 4.0–5.7 ‰). Intragraben post-caldera units have higher $\delta^{18}O$(magma) ($\delta^{18}O$(Zrc) = 1.9–5.9 ‰; $\delta^{18}O$(magma) = 4.2–8 ‰), though the vast majority are low-$\delta^{18}O$ magmas (see Fig. 4). The paucity of oxygen isotope zoning in LOVF zircons can be seen in a plot of $\delta^{18}O(Zrc)_{core}$ vs. $\delta^{18}O(Zrc)_{rim}$ (Fig. 5A). LOVF zircons overwhelmingly cluster tightly on the $\delta^{18}O_{core} = \delta^{18}O_{rim}$ line, and several distinct clusters are suggestive of discrete "magma batches." The spatial and temporal relations within these data are complex, but the individual batches are labeled by number in Fig. 5a and may roughly be associated with (1) the Dinner Creek Tuff, (2) intragraben pre-caldera McIntyre Ridge rhyolites (and the geographically nearby post-caldera Round Mountain), (3) the Tuff of Leslie Gulch and the post-caldera Devil's Gate rhyolite and sanidine rhyolite, (4) intragraben post-caldera rhyolite dikes and Bannock Ridge rhyolite, and (5) the Mahogany Mountain rhyolite. The spatial and temporal significance of these "magma batches" remains speculative, though the data may relate to varying degrees of homogenization within magmas sourcing climactic eruptions, and/or changes in the amount (or $\delta^{18}O$) of assimilated low-$\delta^{18}O$ material in caldera-forming and post-caldera magmatism (Batch 3 and Batch 4). This said, the general homogeneity of units within the LOVF data set, and the relative coherence of these individual units, is striking compared to other centers within the SRP-Y.

The relative homogeneity of $\delta^{18}O$ values in individual LOVF zircons can be contrasted with zoned zircons from rhyolites at Yellowstone, which form subhorizontal trends in Fig. (5c), and are developed particularly well in the post-Lava Creek Tuff lavas (Middle Biscuit Basin, Canyon, and Dunraven flows). These subhorizontal trends in post-caldera Yellowstone zircons, combined with paired U–Pb age data, demonstrated that zircon cores are antecrystic and grew in magmas of variable oxygen isotope composition, while rims grew in a more uniform, low-$\delta^{18}O$ magma or magmas (Bindeman et al. 2001, 2008). For Yellowstone zircons, this supports a model in which zircon cores were inherited from a variety of volcanic and subvolcanic sources with both normal and low $\delta^{18}O$ compositions, and subsequently grew rims during "batch assembly and homogenization" of the post-caldera low-$\delta^{18}O$ magma (Bindeman et al. 2008). This conclusion has been used to support a model in which the genesis of low-$\delta^{18}O$ magmas at Yellowstone is intrinsically related to caldera subsidence (Bindeman et al. 2008). The difference in zonation between LOVF and Yellowstone zircon, the presence of low-$\delta^{18}O$ caldera-forming units in the absence of evidence for nested caldera structures, and the recovery to more normal $\delta^{18}O$ values in post-caldera units in the LOVF suggest that assimilation of low-$\delta^{18}O$ material and incorporation of antecrystic zircon are *not* intrinsically linked to caldera subsidence in the LOVF. As a result, the record of low-$\delta^{18}O$ magmatism in the LOVF is not well explained by caldera subsidence models for low-$\delta^{18}O$ magma genesis.

The relationship between OIG extension and low-$\delta^{18}O$ magmatism offers another explanation for the low-$\delta^{18}O$ magmas in the LOVF in which meteoric hydrothermal alteration originates from the superposition of extensional tectonics and hotspot-derived thermal additions to the crust (Fig. 3e; Blum et al. 2012, 2013; Blum 2013; Colon et al. 2015a, b). Modification of the crustal permeability structure through creation of transient fluid flow pathways associated with normal faulting in the upper crust has been shown to allow migration of low-$\delta^{18}O$ meteoric water to depths up to 10 km within detachment systems (Morrison 1994; Barnett et al. 1996; Losh 1997; Holk and Taylor 1997, 2007, Gottardi et al. 2013; Gébelin et al. 2014; Ingebritsen and Manning 2010). While the OIG is not a detachment system, normal faulting and fracturing associated with the development of OIG horst and graben structures would nonetheless increase crustal permeability, and may allow meteoric fluids to depths where hydrothermal alteration and subsequent assimilation can occur. High, hotspot-derived thermal inputs to the crust would help drive both extension, as well as hydrothermal alteration and subsequent remelting of low-$\delta^{18}O$ rock. While faulting associated with extensional tectonism may also act to displace hydrothermally altered material downward within the crustal column, low-$\delta^{18}O$ caldera-forming magmatism in the LOVF is closely associated with initiation of graben subsidence; as a result, little *vertical* displacement of rock may have occurred prior to eruption of the large-volume Tuff of Leslie Gulch. There are few constraints on the depths and spatial patterns of hydrothermal alteration and magma genesis within the LOVF, and we suggest that the presence of normal-$\delta^{18}O$ magmas is compatible with pervasive, yet heterogeneous, meteoric hydrothermal alteration associated with extensional tectonics.

Based on the data, we cannot explicitly exclude preexisting low-$\delta^{18}O$ regions within the sub-LOVF crust from

**Table 3** Summary of tectonic setting and oxygen isotopes in SRP-Y subregions

| | LOVF | Owyhees | CSRP | Picabo | ESRP |
|---|---|---|---|---|---|
| Centers with $\delta^{18}O$(Zrc) data | Lake Owyhee | Jarbidge Rhyolite | Bruneau-Jarbidge | Picabo | Heise |
| | | Misc. Owyhees (center unknown) | Jim Sage | | Yellowstone |
| Other centers | McDermitt | South Mountain | Twins Falls | | |
| | High Rocks, etc. | | | | |
| Tectonic setting | Accreted Terranes | Transitional/Craton | Craton | Craton | Craton |
| $\delta^{18}O$(Zrc) range | 1.7–6.8 ‰ | −0.6 to 6.6 ‰ | −3.4 to 8.1 ‰ | −0.3 to 6.8 ‰ | −2.2 to 7.6 ‰ |
| Fraction $\delta^{18}O$(Zrc) <4.0 ‰ | 0.636 | 0.583 | 0.968 | 0.604 | 0.815 |
| $\delta^{18}O$ zoning (core–rim) | −1.5 to 0.9 ‰ | – | −2.8 to 3.5 ‰ | – | −3.3 to 6.7 ‰ |
| Extrusive volume of low-$\delta^{18}O$ magma | ~600 $km^3$ | Unknown | >7000 $km^3$ | Unknown | >3000 $km^3$ |
| Low-$\delta^{18}O$ caldera-forming eruptions? | Yes | Unknown | Probable | No | Yes |
| $\delta^{18}O$ response to caldera subsidence | Increase | Unknown | Unknown | Decrease | Decrease |

contributing to low-$\delta^{18}O$ magmas. The geographic distribution of pre-hotspot magmatism (and any associated meteoric hydrothermal alteration) in east-central Oregon is poorly constrained due to cover by younger sediments, rhyolites, and basalts. Magmatism of Eocene to Late Miocene age has been inferred from the general migration of Eocene to Miocene arc magmatism in the Pacific Northwest, and from Oligocene-to-Miocene silicic and calc-alkalic volcanic basement outcrops in northern Nevada, southern Oregon, and southwestern Nevada (Cummings et al. 2000). However, the relationship between LOVF low-$\delta^{18}O$ magmatism and extensional tectonics, combined with other suggestions that extensional tectonics may be important elsewhere in the SRP-Y (Drew et al. 2013), promotes considering the superposition of extension and hotspot magmatism as a more general model for the low-$\delta^{18}O$ magmas of the SRP-Y.

## Oxygen isotopes in SRP-Y magmas

Zircon oxygen isotope data now exist for several units from the majority of SRP-Y centers (Fig. 4c). We have compiled 1553 analyses on 925 zircons from 69 samples (57 different eruptive units) originating from six centers in the greater SRP-Y province. These data provide a robust record of both the high concentration of low-$\delta^{18}O$ magmatism throughout the province and spatiotemporal changes in the magnitude of $^{18}O$ depletions along the hotspot track. All SRP-Y centers have produced low-$\delta^{18}O$ magmas; however, the total volumes, volumetric percentages, and $\delta^{18}O$ trends through time vary along the hotspot track (Boroughs et al. 2012). A general summary of $\delta^{18}O$ trends within the primary subregions of the SRP-Y is given below, as well as in Table 3.

### *LOVF*

The low-$\delta^{18}O$ magmas of the LOVF (16.3–15.4 Ma) have erupted west of the cratonic boundary, lack large degrees of unit-scale zircon $\delta^{18}O$ heterogeneity (<1.5 ‰), and include low-$\delta^{18}O$ large-volume caldera-forming units. Low-$\delta^{18}O$ magmas postdate initiation of OIG subsidence and reside spatially within the OIG. The relative increase in $\delta^{18}O$(magma) between caldera-forming and post-caldera units is antithetical to the rapid decreases in $\delta^{18}O$(magma) associated with caldera subsidence trends (e.g., Watts et al. 2011). There is no known source of preexisting low-$\delta^{18}O$ crust within the region.

### *CSRP*

The Central Snake River Plain (CSRP; 13.0 to ~7 Ma) contains greater than 7000 $km^3$ of low-$\delta^{18}O$ magmas which erupted within the North American craton (Boroughs et al. 2005, 2012; Bonnichsen et al. 2008; Cathey et al. 2008; Seligman 2012; Colon et al. 2015b). In addition, early (> 15 Ma) normal-$\delta^{18}O$ rhyolites exist within the JP Desert (Colon et al. 2015b); however, the relation of these rhyolites to the CSRP is unclear because (1) they precede the main phase of CSRP volcanism by >2 million years and (2) they are geochemically distinct from the adjacent CSRP rhyolites (Burseke et al. 2014). Thus, their connection to CSRP and greater SRP-Y hotspot volcanism is questionable (Burseke et al. 2014; Colon et al. 2015b). The main phase of CSRP rhyolites possess zircons crystallized almost exclusively from low-$\delta^{18}O$ magmas, with little evidence for significant normal-$\delta^{18}O$ magmatism. Zircons possess large degrees of core–rim, and intergrain $\delta^{18}O$ heterogeneity. These centers also include low-$\delta^{18}O$ large-volume units

(Cathey et al. 2008), though $\delta^{18}O$ trends between presumed caldera-forming and post-caldera units are ambiguous given the current level of mapping and exposure. Meteoric hydrothermal alteration by Eocene intrusives is proximal to the CSRP. Zircons possess large degrees of core–rim, and intergrain $\delta^{18}O$ heterogeneity (Cathey et al. 2008; Seligman 2012). Meteoric hydrothermal alteration by Eocene intrusives is proximal to the CSRP.

*ESRP*

The Eastern Snake River Plain (ESRP; less than ~8 Ma) contains greater than 3000 $km^3$ of low-$\delta^{18}O$ magmas, erupted on the North American craton. Low-$\delta^{18}O$ units are generally restricted to post-climatic intracaldera volcanism, or late-stage ignimbrites, though some notable exceptions occur (e.g., Mesa Falls Tuff in the Yellowstone center). ESRP zircons possess varying degrees of intragrain, and intergrain $\delta^{18}O$ heterogeneity. Caldera-forming units have more homogeneous zircons, while post-caldera zircons contain large degrees of intergrain and intragrain variability. Many units, particularly those erupted immediately after caldera subsidence, contain subpopulations with more uniform low-$\delta^{18}O$ rims. There is no evidence supporting preexisting low-$\delta^{18}O$ crust within the ESRP. We note that the high fraction of $\delta^{18}O$(Zrc) <4.0 ‰ (Table 3) is in part due to the sampling bias favoring analysis of zircons from low-$\delta^{18}O$ units both in Yellowstone (post-Lava Creek Tuff lavas) and in Heise (low-$\delta^{18}O$ Kilgore Tuff and pre-Kilgore Tuff lavas).

These $\delta^{18}O$(Zrc) data are suggestive of several similarities, but also distinct differences between centers. The general constraints on low-$\delta^{18}O$ magmatism from the above descriptions require that the underlying alteration and assimilation processes:

1. Operate in both the craton, *and* in accreted terranes.
2. Account for the complete range in $\delta^{18}O$(Zrc) (−3.4 to 7.6 ‰), and the variability in the $\delta^{18}O$ range from center to center.
3. Account for the total volume of low-$\delta^{18}O$ magma, and differences in low-$\delta^{18}O$ magma volumes between centers.
4. Are consistent with a variety of stratigraphic/temporal evolutions: (e.g., early vs. late onset of low-$\delta^{18}O$ magmatism, decreasing vs. increasing $\delta^{18}O$ in response to caldera subsidence).
5. Are consistent with batch assembly/homogenization processes active throughout the province.

These trends offer varyingly restrictive constraints on low-$\delta^{18}O$ magmatism. An increase in $\delta^{18}O$ in response to caldera subsidence, for example, is antithetical to the lowering trends predicted for models where low-$\delta^{18}O$ magmatism is linked to caldera collapse; as a result, other mechanisms must be active. Conversely, batch assembly and homogenization of antecrystic material may be broadly compatible with multiple alteration patterns. In combining these trends with regional $\delta^{18}O$(magma) and $\delta^{18}O$(WR) relations, this allows for the description of the unique aspects of SRP-Y magmatism, and places further constrains of the petrogenesis of SRP-Y low-$\delta^{18}O$ magmas.

## Oxygen isotopes in the Basin and Range and Idaho batholith

Assessing the viability of general mechanisms for low-$\delta^{18}O$ magma genesis in the SRP-Y, including their number, timing, and spatial extent, is informed though evaluating the uniqueness of the SRP-Y with respect to the surrounding regions. A compilation of whole-rock and zircon data from the Basin and Range and Idaho batholith (Figs. 6, 7) place constraints on (1) the presence/absence of low-$\delta^{18}O$ *magmatism* through time within these regions, (as well as their character, i.e., magnitude of depletions, spatial extent, timing, and duration) relative to the SRP-Y, and (2) the presence/absence of large and pervasive low-$\delta^{18}O$ regions of the crust which may serve as source for low-$\delta^{18}O$ magmatism. Except where otherwise stated, $\delta^{18}O$(magma) is constrained from zircon $\delta^{18}O$ analyses within these compilations.

Given the coupled extensional history of the SRP-Y and Basin and Range (e.g., Rodgers et al. 2002), the most direct comparison for oxygen isotopes in SRP-Y silicic magmatism is ~16 Ma to present silicic magmatism within the Basin and Range. Published oxygen isotope data are available for several volcanic centers including the Valles caldera in New Mexico, the Oasis Valley/Timber Mountain caldera complex (also referred to as the southwest Nevada caldera complex) in southwest Nevada, Long Valley caldera in California, and the Twin Peaks volcanic center in Utah (Figs. 6, 7; see references in Online Resource 6). While zircon $\delta^{18}O$ data are largely unavailable to constrain $\delta^{18}O$(magma) for these centers, the available data are used to assess the presence/absence of volcanic low-$\delta^{18}O$ material within the broader region. These units have a range in calculated whole-rock $\delta^{18}O$ between 5.4 and 11.9 ‰, with the only low-$\delta^{18}O$ units ($\delta^{18}O$(rhyolite) <6.0 ‰) being the Ammonia Tanks Tuff and post-Ammonia Tanks rhyolites of the Oasis Valley/Timber Mountain caldera complex (Bindeman and Valley 2003). Oxygen isotope data are dominated by normal- to high-$\delta^{18}O$ values, a trend that is consistent within older 16–35 Ma eruptive centers for which there are no published low-$\delta^{18}O$ values (Fig. 7e). Despite the lone exception of the Ammonia Tanks Tuff, there is no evidence to suggest widespread and pervasive low-$\delta^{18}O$ magmatism within the Basin and Range within the last ~35 Ma.

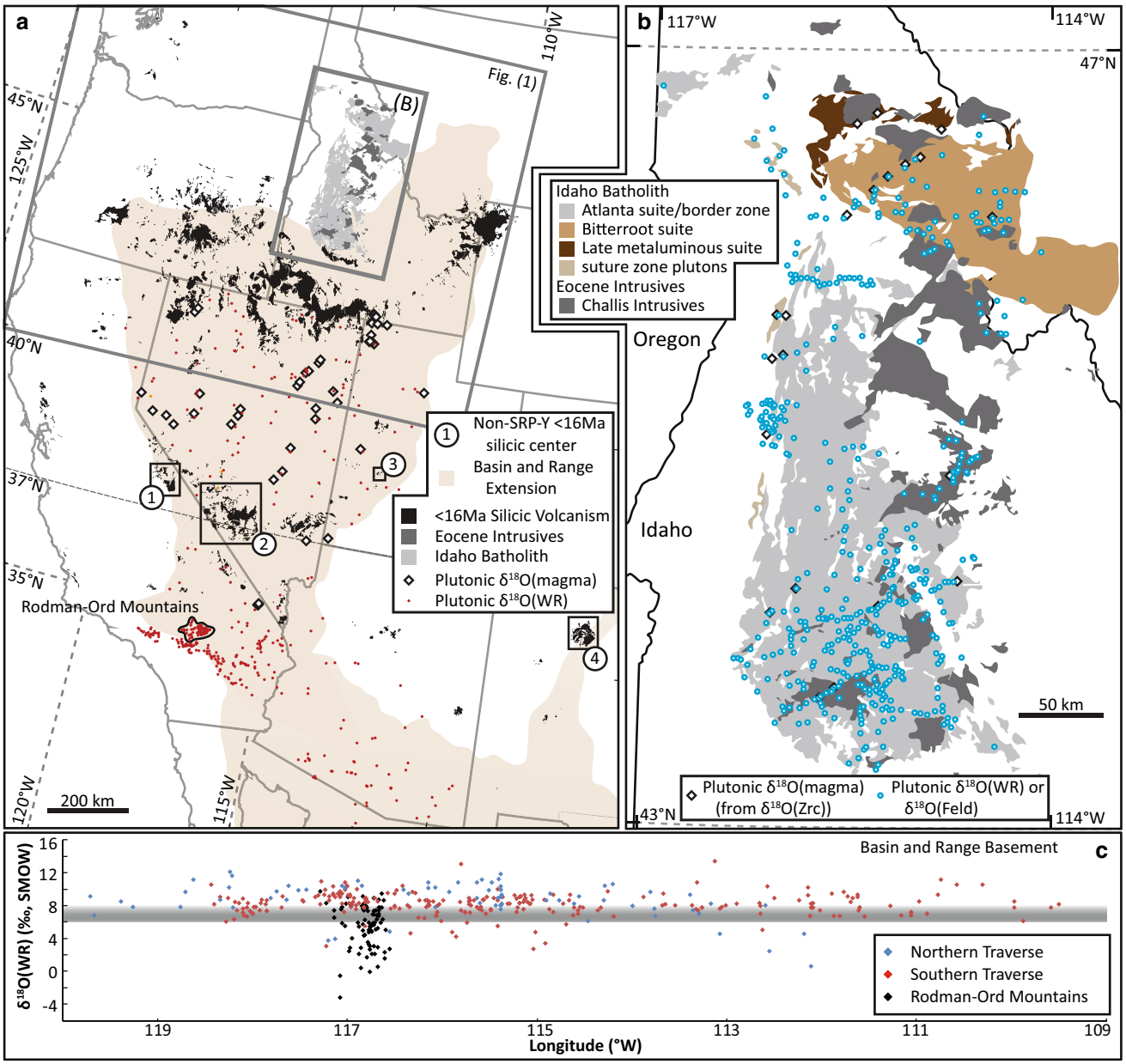


**Fig. 6** **a** Distribution of $\delta^{18}O$(WR) and $\delta^{18}O$(Zrc) samples from 1500 Ma to 23 Ma basement lithologies (granitoids and metamorphic rocks) throughout the Basin and Range, and Idaho batholith. Diamonds are sample locations for $\delta^{18}O$(magma) calculated from zircon, and red points are the location of $\delta^{18}O$(WR) analyses. Location of Figs. 1 and 6b shown in gray outlines. *Boxes* 1–4 refer to volcanic centers in Fig. 7d. **b** Sample locations of $\delta^{18}O$(WR) and $\delta^{18}O$(Zrc) within the Idaho batholith and surroundings. **c** Longitudinal traverses across the Basin and Range province for the data points in **a**. "Northern traverse" includes data north of 37°N latitude, while the "southern traverse" includes data south of 37°N latitude (37°N latitude shown as gray dashed line). See Online Resources 6 and 7 for references and compiled oxygen isotope analyses

This contrasts with the pervasive low-$\delta^{18}O$ magmas of the SRP-Y.

A compilation of whole-rock analyses from plutonic and metamorphic rocks across the Basin and Range, as well as crustal xenoliths within the SRP-Y, allow for further evaluation of the oxygen isotope nature of the crust (Figs. 6, 7; Online Resource 7), particularly in constraining the potential presence/absence of large and pervasive low-$\delta^{18}O$ regions within the Basin and Range. Data for Archean crustal xenoliths within SRP-Y basalts have homogeneous $\delta^{18}O$(WR) values with averages between 6.3 ‰ and 9.3 ‰ (Fig. 7g; Watts et al. 2010), and are consistent with the generally normal- to high-$\delta^{18}O$(WR) values within the Basin and Range. Basin and Range whole-rock analyses

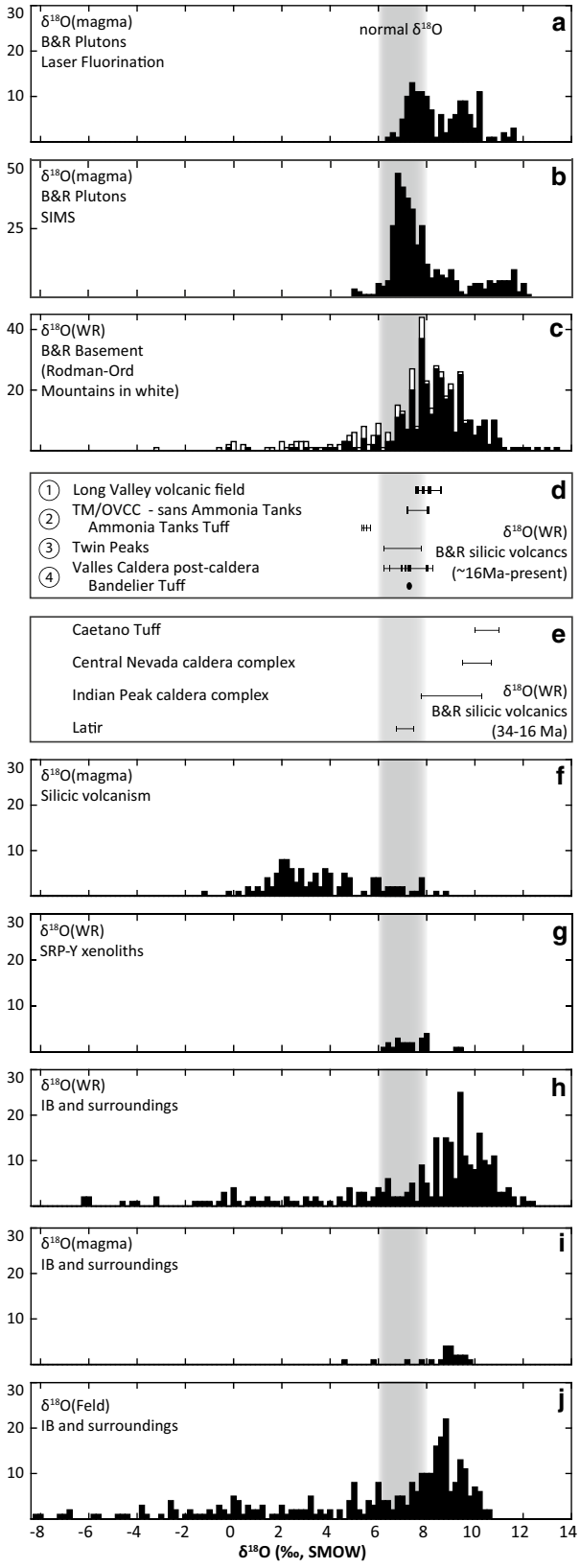


**Fig. 7** $\delta^{18}O$ histograms for magmas (measured, or calculated based on zircon analyses) and measured whole-rocks throughout the SRP-Y and adjacent regions. See Fig. 6 for distribution of samples. **a** $\delta^{18}O$(magma) for Basin and Range plutons calculated from laser fluorination $\delta^{18}O$(Zrc) measurements. **b** $\delta^{18}O$(magma) for Basin and Range plutons calculated from SIMS-based $\delta^{18}O$(Zrc) measurements. **c** $\delta^{18}O$(WR) for Basin and Range plutonic and metamorphic rocks. **d** ~16 Ma to present silicic volcanism throughout the Basin and Range. Numbers correlate with centers in Fig. 6. **f** 34–16 Ma silicic volcanism within the Basin and Range. **f** $\delta^{18}O$(magma) for SRP-Y magmas for individual hand samples. **g** Average $\delta^{18}O$(WR) for xenoliths within CSRP basalts. **h, i, j** $\delta^{18}O$(WR), $\delta^{18}O$(magma), and $\delta^{18}O$(Feldspar) measurements for the Idaho batholith and surroundings. See Online Resources 6 and 7 for data compilation, ages, and references, as well as calculation of magma–zircon fractionations

have $\delta^{18}O$(WR) between −3.2 and +13.4 ‰ (Fig. 7c), and the vast majority (> 83 %) of 448 analyses have normal- to high-$\delta^{18}O$ values (Fig. 7c). Longitudinal traverses show few regions with high concentrations of low-$\delta^{18}O$(WR), the one main exception being the Rodman-Ord mountains of southeast California (Fig. 6c). The origin of low-$\delta^{18}O$ rocks within the Rodman-Ord mountains is unresolved; however, low-$\delta^{18}O$ Proterozoic zircons ($\delta^{18}O$(Zrc) = 3.3–4.6 ‰) from gneisses within the Rodman-Ord mountains indicate that alteration predates, and is thus unrelated to, Basin and Range extension (Zilberfarb et al. 2012). The whole-rock data set for the entire Basin and Range suggests that oxygen isotope anomalies similar to those in the Rodman-Ord Mountains are not widespread, and are not related to the extensional tectonics of the present-day Basin and Range. This is further supported by the absence of low-$\delta^{18}O$ *magmatism* in plutons from the northern portion of the Basin and Range as constrained by zircon $\delta^{18}O$ analyses (Fig. 7a, b). Zircon data for plutons with ages from 1500 Ma to 28 Ma record $\delta^{18}O$(magma) values (calculated from zircon, excluding Rodman-Ord Mountains) between 6.4 ‰ to 11.7 ‰, placing them in the normal- to high-$\delta^{18}O$(magma) range. Thus, these magmas do not record assimilation of low-$\delta^{18}O$ material and provide no evidence in favor of pervasive, long-standing regions of low-$\delta^{18}O$ crust within the Basin and Range, and sub-SRP-Y crust.

Within the Cretaceous Idaho batholith, *magmatism* is dominated by normal-$\delta^{18}O$ values (Fig. 7i). Eocene alteration by meteoric waters has *locally* generated $\delta^{18}O$(Fsp) and $\delta^{18}O$(WR) values as low as −8.2 ‰ (Criss and Taylor 1983; Criss et al. 1984; Fig. 7h, j). Values of $\delta^{18}O$(WR) are highly variable over short distances (10′s to 100′s of meters), and are consistent with alteration originating from locally channelized flow. Overall, the predominantly normal- to high-$\delta^{18}O$(WR) and $\delta^{18}O$(Fsp) values from the

Idaho batholith (Fig. 7h–j) are indicative of either magmatic values or low temperature alteration, and do not support the assertion that low-$\delta^{18}O$ alterations zones are widespread and pervasive. These studies are all demonstrative of *regions* of low-$\delta^{18}O$ material; however, their pervasiveness, continuity, and extent remain inconclusive.

We note that in the case of high-$\delta^{18}O$ initial whole-rock values, meteoric hydrothermal alteration may not lower $\delta^{18}O$(WR) into the <6.0 ‰ range discussed in the paper; as a result, assimilation of such hydrothermally altered material would appear as a *relative* lowering in $\delta^{18}O$(magma), but would not produce $\delta^{18}O$(magma) values below mantle-like values. This is important in considering weather regional differences in initial $\delta^{18}O$(WR) may obscure otherwise similar hydrothermal alteration and assimilation patterns between the SRP-Y and adjacent regions. In the context of this study, we are primarily concerned with the origin and distribution of low-$\delta^{18}O$ rocks which may serve as a low-$\delta^{18}O$ assimilant for SRP-Y low-$\delta^{18}O$ rhyolites. The regional record of $\delta^{18}O$ summarized within Figs. 6 and 7 does not support the idea of a widespread, regionally extensive low-$\delta^{18}O$ source region equivalent to that contributing to SRP-Y magmatism. While we do not attempt a thorough review of $\delta^{18}O$(WR) for *all* lithologies throughout the region, we note that there is a first-order similarity in $\delta^{18}O$(WR) for the presumptive basement lithologies both in the SRP-Y (i.e., SRP-Y xenoliths) and in Basin and Range and Idaho batholith (Fig. 7). These data support the idea that there are distinct differences in the *recent* (<16 Ma) alteration and assimilation histories for magmas within these areas. This said, relatively few centers within the Basin and Range are well studied with respect to $\delta^{18}O$. The in-depth study of $\delta^{18}O$ and emplacement relations within Basin and Range volcanic centers would help elucidate the nature of any relative $\delta^{18}O$ shifts, and how such shifts relate to structural and tectonic associations.

To summarize, the compilation of oxygen isotope data (Figs. 6 and 7) from the Idaho batholith/Challis intrusives demonstrates the lack of low-$\delta^{18}O$ magmas within the Idaho batholith as well as the limited extent of low-$\delta^{18}O$ magmas within related Eocene intrusions, and the moderate areal extent of $^{18}O$-depleted rock associated with hydrothermal alteration by Eocene intrusions. Oxygen isotope data from across the Basin and Range support three major conclusions: (1) volcanism over the last 35 Ma is dominated by normal- to high-$\delta^{18}O$ ($\delta^{18}O$(WR) >6 ‰), (2) low-$\delta^{18}O$ magmas are rare prior to the Early Miocene, and (3) the majority of Basin and Range crust is represented by normal- to high-$\delta^{18}O$(WR) values. The $\delta^{18}O$ values of xenoliths (Watts et al. 2010) further demonstrate the small areal extent of pervasive low-$\delta^{18}O$(WR) regions in the Basin and Range and Idaho batholith, and demonstrate the *regional uniqueness of SRP-Y low-$\delta^{18}O$ magmatism*. These observations highlight the strength of models for low-$\delta^{18}O$ magma genesis that account for the unique thermal and structural evolution of SRP-Y centers.

## Models for the genesis of SRP-Y low-$\delta^{18}O$ magmas

Similar to the associations within the LOVF, there exist general observations which must be explained by any holistic model for low-$\delta^{18}O$ SRP-Y magma genesis. These include (1) oxygen isotope trends within individual eruptive centers, (2) along axis trends in oxygen isotopes for felsic magmas within the hotspot track (Fig. 4), and (3) the high volumetric concentration of low-$\delta^{18}O$ magmas and the magnitude of $\delta^{18}O$ lowering, relative to the surrounding regions.

### *Preexisting low-$\delta^{18}O$ source*

Whole-rock and zircon oxygen isotope data from north of the SRP demonstrate (1) the lack of low-$\delta^{18}O$ magmas in the Idaho batholith, and relative rarity of low-$\delta^{18}O$ magmas within related Eocene intrusions, and (2) that low-$\delta^{18}O$ rock associated with hydrothermal alteration by Eocene intrusions (see discussion in previous section) is not both widespread and pervasive. The largest, well-defined alteration zones within the Idaho batholith are on the order of 50 km in diameter. In order to account for the >7000 $km^3$ of low-$\delta^{18}O$ CSRP volcanic products, this model for low-$\delta^{18}O$ magmatism would require that (1) large regions of low-$\delta^{18}O$ rock existed within these caldera systems that is unobserved, and (2) the size, and/or density of Eocene systems was distinctly greater in the sub-CSRP crust relative to that exposed to the adjacent Idaho batholith. More pervasive low-$\delta^{18}O$ hydrothermal alteration zones have been hypothesized to exist in the absence of data in the now-eroded intracaldera blocks within the aforementioned Eocene caldera systems (Boroughs et al. 2012). We note that the lower portions of the exposed sections of well-studied systems (e.g., Lake City caldera; Larson and Taylor 1986) contain sharp $\delta^{18}O$ gradients over short distances (10′s to 100′s of meters), similar to those in the Eocene caldera systems of the Idaho batholith. Given this, the inferred volume of low-$\delta^{18}O$ material in an intracaldera block is highly dependent upon interpolations between distant samples in domains with poor sample coverage and variable lithologies. The limitations of this model are compounded by the spatially distant low-$\delta^{18}O$ magmas. Given that these LOVF and ESRP magmas lie well removed from the low-$\delta^{18}O$ exposures within the Idaho batholith, an independent model/source region and pattern of alteration is necessary to explain the occurrence of low-$\delta^{18}O$ magmas.

Oxygen isotope data from across the Basin and Range show (1) the relative paucity of low-$\delta^{18}O$ magmatism throughout the region's history into the Early Miocene, (2) no evidence for systematic low-$\delta^{18}O$(WR) regions within the Basin and Range crust (on the scale of the SRP), and (3) that volcanism over the last 35 Ma is dominated by normal- to high-$\delta^{18}O$ phenocryst and whole-rock values. These observations argue against models that do not distinguish between the permeability *and thermal* structure of the SRP-Y and that of the surrounding Basin and Range province. Alteration models which utilize general crustal-scale permeability relations (Leeman et al. 2008) imply that there exists a uniform and pervasive low-$\delta^{18}O$ layer within the crust that is extensive in both time and space, as the modeled thermal and permeability state is not limited to the last ~16 Ma, or solely to the SRP-Y. There is no evidence for such a large and extensive feature, and as a result, this type of deep, protracted fluid circulation and $\delta^{18}O$ lowering of the crust is considered unlikely as an explanation for the low-$\delta^{18}O$ magmatism of the SRP-Y.

*Caldera subsidence*

As discussed previously for LOVF magmatism, there is no evidence for nested caldera structures prior to low-$\delta^{18}O$ caldera-forming magmatism (in contrast to Yellowstone), and the relative increase in $\delta^{18}O$ between caldera and post-caldera units is antithetical to those inherent in the caldera subsidence model proposed for Yellowstone (Bindeman and Valley 2000, 2001). In addition, the CSRP hosts over 7000 $km^3$ of rhyolitic volcanic products and contain no evidence for significant volumes of normal-$\delta^{18}O$ magma preceding low-$\delta^{18}O$ magmatism (Boroughs et al., 2005, 2012; Cathey et al. 2008; Seligman 2012). Given the data and trends outlined above, we conclude that the caldera subsidence model does not fully explain low-$\delta^{18}O$ magma genesis within the greater SRP-Y. However, elements of this model capture general relations in the generation and subsequent assimilation of low-$\delta^{18}O$ rock. In this model, meteoric hydrothermal circulation and alteration is associated with silicic hotpot magmatism, and is likely controlled, at least in part, by fracture/fault networks associated with caldera collapse and deformation surrounding the evolving magmatic system. Caldera subsidence introduces low-$\delta^{18}O$ rock to depth where adjacent magma can assimilate it, and while this *specific* subsidence mechanism limits application to the broader SRP-Y province, the general association between alteration, subsidence, and assimilation captured in this model can be generalized in a separate model which can explain the oxygen isotope associations throughout the SRP-Y.

*Hotspot magmatism and extensional tectonics*

Many of the SRP-Y centers (including the LOVF) reside in tectonic settings where magmatic and structural histories potentially preserve a balance between syn-hotspot hydrothermal alteration, normal faulting and subsidence, and subsequent melting/assimilation (Taylor 1986; Blum et al. 2012, 2013; Drew et al. 2013; Colon et al. 2015a, b). Analogous to extension, normal faulting and magmatism in the LOVF, the CSRP and ESRP are superimposed on the actively extending Basin and Range as evidenced by (1) the existence of Basin and Range style extension within and proximal to the pre-hotspot SRP-Y (both north and south), (2) the coupled Miocene to present extension of the Snake River Plain and adjacent Basin and Range, and (3) the increased extension rate along Basin and Range faults directly adjacent to the SRP coincident with the onset of magmatism at a given center (Anders et al. 1989; Rodgers et al. 1990; Pierce and Morgan 1992; Parsons et al. 1998; Rodgers et al. 2002). In the case of the SRP-Y, we propose that the thermal influence of hotspot magmatism, superimposed on Basin and Range extensional tectonics, generates a permeability structure and thermal driving force to produce large-volume low-$\delta^{18}O$ regions of the crust, which are then subsequently incorporated into SRP-Y silicic magmas. This model is compatible with two first-order trends in the $\delta^{18}O$(magma) evolution for the SRP-Y: (1) the differences between the SRP-Y and surrounding regions, and (2) the genesis of low-$\delta^{18}O$ magmas in the absence of (and/or predating) nested caldera structures, as is observed in the LOVF and CSRP. The distribution and timing of extensional tectonics is also consistent with the operation of this mechanism in both cratonic and accreted terranes. This general model remains compatible with a variety of $\delta^{18}O$ trends within individual eruptive centers, $\delta^{18}O$ zoning trends, and volumes of low-$\delta^{18}O$ magmas. The local geology and variable nature of primary hotpot thermal fluxes on timescales of $10^4$ to $10^6$ years (Perkins and Nash 2002), as well as the intricacies of extensional, structural, and permeability relations, may explain the center-to-center variability in volume of low-$\delta^{18}O$ magmas in the SRP-Y. Even within Yellowstone, where low-$\delta^{18}O$ rhyolites are highly correlated with caldera subsidence, NNW–SSE-trending faults are common within and adjacent to the Yellowstone caldera (Christiansen 2001), and these faults may remain active as fluid conduits, while other subsidence mechanisms (i.e., caldera subsidence) exhibit a geometric control over the burial of low-$\delta^{18}O$ material, and are thus a prominent control on the oxygen isotope evolution of ESRP magmas.

While the enhancement of crustal-scale permeability by normal faults and deep localized penetration of meteoric

water during extension are well documented (Muir-Wood and King 1993; Morrison 1994; Barnett et al. 1996; Losh 1997; Holk and Taylor 1997, 2007, Gottardi et al. 2013; Gébelin et al. 2014; Ingebritsen and Manning 2010), none of these studies demonstrate volumetrically extensive and pervasive (over 100′s of meters) low-$\delta^{18}O$ regions within the crust extending appreciably outside fracture zones. This, as well as the $\delta^{18}O$(WR) data for the greater Basin and Range (Fig. 7c), is consistent with the lack of large regions of low-$\delta^{18}O$ rock and magmas within the Basin and Range as documented above, and both of these observations argue against models where hydrothermal alteration is driven *solely* by advection of heat during metamorphic core complex formation (Konstantinou et al. 2013; Drew et al. 2013).

Boroughs et al. (2012) argue that energy balance considerations prevent syn-hotspot hydrothermal alteration and significant melting of the crust from operating without geologically unreasonable volumes and intrusion rates for mantle-derived magmas. Although meteoric hydrothermal alteration unquestionably acts as an energy sink, thermal modeling incorporates significant uncertainties in estimating total magma volumes, emplacement depths, emplacement rates, periodic melt extraction, and spatial accommodation mechanisms (Bonnichsen et al. 2008; Leeman et al. 2008; Rodgers and McCurry 2009; Simakin and Bindeman 2012). The magnitude and duration of magma fluxes appropriate to generate mid- to shallow-crustal silicic magmas are also incompletely resolved, as are the compositions of the assimilated crustal component (i.e., "melt fraction vs. temperature relationship," of Gelman et al. (2013)), emplacement rates, temperature dependence of thermal diffusivity (Whittington et al. 2009), and geothermal gradients all influence the composition and volume of eruptible material, as well as the longevity of melt within a system (Leeman et al. 2008; Simakin and Bindeman 2012; Annen 2009; Gelman et al. 2013). Given the uncertainty in thermal models for the SRP-Y centers, we conclude that syn-hotspot timing for alteration cannot be excluded solely on the basis of energy balance considerations. We argue that the ability of syn-hotspot alteration to account for the uniqueness of the entire SRP-Y relative to adjacent regions suggests syn-hotspot magmatism is the dominant process controlling the timing and magnitude of alteration that sourced the low-$\delta^{18}O$ magmas of the SRP-Y.

### Low-$\delta^{18}O$ large igneous provinces

The model presented here may be applied too other low-$\delta^{18}O$ igneous provinces such as Tongbai-Dabie-Sulu (TDS, e.g., Wang et al. 2011; Fu et al. 2012), and the North Atlantic igneous province (NAIP; includes the British Tertiary Igneous Province, Iceland, e.g., Taylor and Sheppard 1986; Monani and Valley 2001; Bindeman et al. 2011), where similar thermal and structural relations existed in the geological past. The structural settings, the presence of high thermal inputs from the mantle, and the presence of volumetrically significant low-$\delta^{18}O$ magmatism are well documented, and indicate the presence of high mantle-derived thermal inputs superimposed on extensional tectonics. While low-$\delta^{18}O$ magmatism also occurs outside of rift settings, the similarity in tectonic and thermal settings between the SRP-Y, NAIP, and TDS suggests that the general model presented above is the most common mechanism for generating *province-scale* volumes of low-$\delta^{18}O$ magmas. This conclusion has implications for the broader application of $\delta^{18}O$ analysis within detrital zircons. *Primary* $\delta^{18}O$ values are valuable in elucidating tectonic associations and sediment provenance; low-$\delta^{18}O$ zircons in particular may provide useful supporting evidence for rifting environments. Alternatively, if the source rock(s) for low-$\delta^{18}O$ zircons is known, they may act as diagnostic provenance indicators. This has been demonstrated indirectly within TDS (Wang et al. 2011), and may be further explored in sedimentary basins sourced by material from low-$\delta^{18}O$ provinces.

## Conclusions

The SRP-Y igneous province hosts >10,000 $km^3$ of low-$\delta^{18}O$ silicic volcanic rocks, and has erupted the largest known volume of low-$\delta^{18}O$ magmas on Earth. The observed magmatic oxygen isotope variability in the SRP-Y is the result of both the crustal-scale thermal and permeability relations that controlled the timing and depth for surface water to penetrate and alter large volumes of the mid-crust, as well as the complexities of melting large portions of the pre-SRP crust. The oxygen isotope trends preserved in zircons from the SRP-Y hotspot track document the presence of low-$\delta^{18}O$ magmas throughout the province, as well as a variety of magmatic $\delta^{18}O$ trends through time and zoning relations. The genesis of these magmas is best explained by the circulation of meteoric water driven by the thermal influence of the hotpot, and facilitated by the crustal-scale permeability structure generated by extensional Basin and Range tectonics. Large-scale alteration driven by the superposition of hotspot-derived thermal inputs and crustal extension is the only model for SRP-Y low-$\delta^{18}O$ genesis which can explain (1) oxygen isotope trends within individual eruptive centers, (2) along axis trends in oxygen isotopes within the hotspot track, and (3) the high concentration of low-$\delta^{18}O$ magmas and the magnitude of $\delta^{18}O$ lowering, relative to the surrounding regions. The fundamental thermal and tectonic associations preserved in the SRP-Y are found in other low-$\delta^{18}O$ igneous provinces such as the North Atlantic igneous province

and Tongbai-Dabie-Sulu, and thus are suggestive of a general model for the province-scale production of low-$\delta^{18}O$ magmas.

**Acknowledgments** We thank Matt Ledvina for assistance in the field, Brian Hess for his contributions to thin section and SIMS mount preparation, and Mark Pecha, N. Geisler, and Intan Yokelson for their help with LA-ICP-MS sample preparation and analysis. We thank K Watts and an anonymous reviewer for constructive reviews which helped improve the quality of this manuscript. This project received financial support for fieldwork from Sigma Xi GIAR (Grant ID G20120315160845), and GSA Graduate Student Research Grant. This research was funded by the US National Science Foundation (EAR-1144454) and the US Department of Energy Office of Science, Office of Basic Energy Sciences, Chemical Sciences, Geosciences, and Biosciences under Award Number DE-FG02-93ER14389. WiscSIMS is partly supported by the US National Science Foundation (EAR-1355590), as is the University of Arizona LaserChron Lab (EAR-1338583).

## References

Anders MH, Geissman JW, Piety LA, Sullivan JT (1989) Parabolic distribution of circumeastern Snake River Plain seismicity and latest Quaternary faulting: migratory pattern and association with the Yellowstone hotspot. J Geophys Res 94:1589–1621

Annen C (2009) From plutons to magma chambers: thermal constrains on the accumulation of eruptible silicic magma in the upper crust. Earth Planet Sci Lett 284:409–416

Armstrong RL, Taubeneck WH, Hales PO (1977) Rb-Sr and K-Ar geochronometry of Mesozoic granitic rocks and their Sr isotopic composition, Oregon, Washington, and Idaho. Bull Geol Soc Am 88:397–411

Barnett DE, Bowman JR, Bromley C, Cady C (1996) Kinetically limited isotope exchange in a shallow level normal fault, Mineral Mountains, Utah. J Geophys Res 101:673–685

Benson TR, Mahood GA (2016) Geology of the Mid-Miocene Rooster Comb Caldera and Lake Owyhee Volcanic Field, eastern Oregon: silicic volcanism associated with Grande Ronde flood basalt. J Volcanol Geoth Res 309:96–117

Bindeman IN (2008) Oxygen isotopes in mantle and crustal magmas as revealed by single crystal analyses. Rev Mineral Geochem 69:445–478

Bindeman IN, Serebryakov NS (2011) Geology, petrology and O and H isotope geochemistry of remarkably $^{18}O$ depleted Paleoproterozoic rocks of the Belomorian Belt, Karelia, Russia, attributed to global glaciation 2.4 Ga. Earth Planet Sci Lett 306:163–174

Bindeman IN, Valley JW (2000) Formation of low-$\delta^{18}O$ rhyolites after caldera collapse at Yellowstone, Wyoming, USA. Geology 28:719–722

Bindeman IN, Valley JW (2001) Low-$\delta^{18}O$ Rhyolites from Yellowstone: magmatic Evolution Based on Analyses of Zircons and Individual Phenocrysts. J Petrol 42:1491–1517

Bindeman IN, Valley JV (2003) Rapid generation of both high- and low-$\delta$ $^{18}O$, large-volume silicic magmas at the Timber Mountain/Oasis Valley caldera complex, Nevada. Geol Soc Am Bull 115:581–595

Bindeman IN, Valley JW, Wooden JL, Persing HM (2001) Post-caldera volcanism: in situ measurement of U-Pb age and oxygen isotope ratio in Pleistocene zircons from Yellowstone caldera. Earth Planet Sci Lett 189:197–206

Bindeman IN, Ponomareva VV, Bailey JC, Valley JW (2004) Volcanic arc of Kamchatka: a province with high-$\delta^{18}O$ magma sources and large-scale $^{18}O/^{16}O$ depletion of the upper crust. 68:841–865

Bindeman IN, Watts KE, Schmitt AK, Morgan LA, Shanks PWC (2007) Voluminous low $\delta^{18}O$ magmas in the late Miocene Heise volcanic field, Idaho: implications for the fate of Yellowstone hotspot calderas. Geology 35:1019–1022

Bindeman IN, Fu B, Kita NT, Valley JW (2008) Origin and evolution of silicic magmatism at yellowstone based on ion microprobe analysis of isotopically zoned zircons. J Petrol 49:163–193

Bindeman IN, Gurenko A, Carley T, Miller C, Martin E, Sigmarsson O (2011) Silicic magma petrogenesis in Iceland by remelting of hydrothermally altered crust based on oxygen isotope diversity and disequilibria between zircon magma with implications for MORB. Terra Nova 24:227–232

Black LP, Kamo SL, Allen CM, Davis DW, Aleinikoff JN, Valley JW, Mundil R, Campbell IH, Korsch RJ, Williams IS, Foudoulis C (2004) Improved $^{206}Pb/^{238}U$ microprobe geochronology by the monitoring of a trace-element-related matrix effect; SHRIMP, ID-TIMS, ELA-ICP-MS and oxygen isotope documentation for a series of zircon standards. Chem Geol 205:115–140

Blum TB (2013) Oxygen isotope evolution of the Lake Owyhee volcanic field, Oregon, and implications for the evolution of the Snake River Plain-Yellowstone low-$\delta^{18}O$ large igneous province. MS Thesis, University of Wisconsin-Madison

Blum TB, Strickland A, Valley JW (2012) Oxygen Isotope Character of the Lake Owyhee Volcanic Field, Oregon. In: Abstract V13B-2845 presented at 2012 Fall Meeting, AGU, San Francisco, 3–7 December

Blum TB, Kitajima K, Nakashima D, Valley JW (2013) Oxygen isotope evolution of the Lake Owyhee volcanic field, Oregon, and implications for low-$\delta^{18}O$ magmas of the Snake River Plain – Yellowstone hotspot. Abstract V33C-2757 presented at 2013 Fall Meeting, AGU, San Francisco, 9–13 December

Bonnichsen B, Leeman WP, Honjo N, McIntosh WC, Godchaux MM (2008) Miocene silicic volcanism in southwestern Idaho: geochronology, geochemistry, and evolution of the central Snake River Plain. Bull Volc 70:315–342

Boroughs S, Wolff J, Bonnichsen B, Godchaux MM, Larson PB (2005) Large-volume, low-$\delta^{18}O$ rhyolites of the central Snake River Plain, Idaho, USA. Geology 33:821–824

Boroughs S, Wolff JA, Ellis BS, Bonnichsen B, Larson PB (2012) Evaluation of models for the origin of Miocene low-$\delta^{18}O$ rhyolites of the Yellowstone/Columbia River Large Igneous Province. Earth Planet Sci Lett 313–314:45–55

Bowman JR, Moser DE, Valley JW, Wooden JL, Kita NT, Mazdab FK (2011) Zircon U-Pb isotope, $\delta^{18}O$ and trace element response to 80 m.y. of high temperature metamorphism in the lower crust: sluggish diffusion and new records of Archean craton formation. Am J Sci 311:719–772

Burseke ME, Callicoat JS, Hames W, Larson PB (2014) Mid-Miocene rhyolite volcanism in northeastern Nevada: the Jarbidge Rhyolite and its relationship to the Cenozoic evolution of the northern Great Basin (USA). Geol Soc Am Bull 126:1047–1067

Camp VE, Hanan BB (2008) A plume-triggered delamination origin for the Columbia River Basalt Group. Geosphere 4:480–495

Camp VE, Ross ME (2004) Mantle dynamics and genesis of mafic magmatism in the intermontane Pacific Northwest. J Geophys Res 109:B08204

Cathey HE, Nash BP, Allen CM, Campbell IH, Valley JW, Kita N (2008) U-Pb zircon geochronology and Ti-in zircon thermometry of large volume low-$\delta^{18}O$ magmas of the Miocene Yellowstone hotspot. Geochim Cosmochim Acta 72:12S–A143

Cherniak DJ, Watson EB (2003) Diffusion in Zircon. Rev Mineral Geochem 53:113–143

Christiansen RL (2001) Geology of Yellowstone National Park – The Quaternary and Pliocene Yellowstone Plateau Volcanic Field of Wyoming, Idaho and Montana. U.S. Geological Survey Professional Paper 729-G

Clayton RN, Goldsmith JR, Mayeda TK (1989) Oxygen isotope fractionation in quartz, albite, anorthite and calcite. Geochim Cosmochim Acta 53:725–733

Coble MA, Mahood GA (2012) Initial impingement of the Yellowstone plume located by widespread silicic volcanism contemporaneous with Columbia River flood basalts. Geology 40:655–658

Colon DP, Bindeman IN, Stern RA, Fisher CM (2015a) Isotopically diverse rhyolites coeval with the Columbia River Flood Basalts: evidence for mantle plume interaction with the continental crust. Terra Nova 27:270–276

Colon DP, Bindeman IN, Ellis BS, Schmitt AK, Fisher CM (2015b) Hydrothermal alteration and melting of the crust during the Columbia River Basalt-Snake River Plain transition and the origin of low-$\delta^{18}O$ rhyolites of the central Snake River Plain. Lithos 224–225:310–323

Criss RE, Taylor HP (1983) An $^{17}O/^{16}O$ and D/H study of tertiary hydrothermal systems in the southern half of the Idaho batholith. Geol Soc Am 94:640–663

Criss RE, Ekren EB, Hardyman RF (1984) Casto Ring Zone: a 4,500-$km^2$ fossil hydrothermal system in the Challis Volcanic Field, central Idaho. Geology 12:331–334

Cummings ML, Evans JG, Ferns ML, Lees KR (2000) Stratigraphic and structural evolution of the middle Miocene synvolcanic Oregon-Idaho graben. Geol Soc Am Bull 112:668–682

Darold A, Humphreys E (2013) Upper mantle seismic structure beneath the Pacific Northwest: a plume-triggered delamination origin for the Columbia River flood basalt eruptions. Earth Planet Sci Lett 365:232–242

Drew DL, Bindeman IN, Watts KE, Schmitt AK, Fu B, McCurry M (2013) Crustal-scale recycling in caldera complexes and rift zones along the Yellowstone hotspot track: o and Hf isotopic evidence in diverse zircons from voluminous rhyolites of the Picabo volcanic field, Idaho. Earth Planet Sci Lett 381:63–77

Evans JG (1996) Geologic Map of the Monument Peak Quadrangle, Malheur County, Oregon, U.S. Geological Survey, MF-2317, scale 1:24,000

Ferns ML (1988) Geology and Mineral Resources Map of the Owyhee Ridge Quadrangle Malheur County, Oregon, State of Oregon Department of Geology and Mineral Industries Geological Map Series, GMS-53, scale 1:24,000

Ferns ML, McClaughry JD (2013) Stratigraphy and evolution of the middle Miocene to Pliocene La Grande-Owyhee eruptive axis in eastern Oregon. Geol Soc Am Spec Pap 497:401–427

Ferns ML, Brooks HC, Evans JG, Cummings ML (1993a) Geologic Map of the Vale 30x60 Minute Quadrangle, Malheur County Oregon, and Owyhee County Idaho, State of Oregon Department of Geology and Mineral Industries, GMS-77, scale 1:100,000

Ferns ML, Evans JG, Cummings ML (1993b) Geologic Map of the Mahogany Mountain 30x60 Minute Quadrangle, Malheur County, Oregon, and Owyhee County, Idaho, State of Oregon Department of Geology and Mineral Industries, GMS-78, scale 1:100,000

Fouch MJ (2012) The Yellowstone Hotspot: plume or Not? Geology 40:479–480

Friedman I, Lipman PW, Obradovich JD, Gleason JD, Christiansen RL (1974) Meteoric water in magmas. Science 184:1069–1072

Fu B, Kita NT, Wilde SA, Liu X, Cliff J, Greig A (2012) Origin of the Tongbai-Dabie-Sulu Neoproterozoic low-$\delta^{18}O$ igneous province, east-central China. Contrib Miner Petrol 165:641–662

Gébelin A, Teyssier C, Heizler MT, Mulch A (2014) Meteoric water circulation in a rolling-hinge detachment system (northern Snake Range core complex, Nevada). Geol Soc Am Bull 127:149–161

Gehrels G, Valencia V, Ruiz J (2008) Enhanced precision, accuracy, efficiency, and spatial resolution of U-Pb ages by laser ablation-multicollector-inductively coupled plasma-mass spectrometry. Geochem Geophys Geosyst 9:Q03017

Gelman SE, Gutierrez FJ, Bachmann O (2013) On the longevity of large upper crustal silicic magma reservoirs. Geology 41:759–762

Gottardi R, Kao PH, Saar MO, Teyssier C (2013) Effects of permeability fields on fluid, heat, and oxygen isotope transport in extensional detachment systems. Geochem Geophys Geosyst 14:1493–1522

Hildreth W, Halliday AN, Christiansen RL (1991) Isotopic and chemical evidence concerning the genesis and contamination of basaltic and rhyolitic magma beneath the Yellowstone plateau volcanic field. J Petrol 32:63–138

Holk GJ, Taylor HP (1997) $^{18}O/^{16}O$ homogenization of the middle crust during anatexis: the Thor-Odin metamorphic core complex, British Columbia. Geology 25:31–34

Holk GJ, Taylor HP (2007) $^{18}O/^{16}O$ Evidence for Contrasting Hydrothermal Regimes Involving Magmatic and Meteoric-Hydrothermal Waters at the Valhalla Metamorphic Core Complex, British Columbia. Econ Geol 102:1063–1078

Ingebritsen SE, Manning CE (1999) Geological implications of a permeability-depth curve for continental crust. Geology 27:1107–1110

Ingebritsen SE, Manning CE (2010) Permeability of the continental crust: dynamic variations inferred from seismicity and metamorphism. Geofluids 10:193–205

Johnson DM, Hooper PR, Conrey RM (1999) XRF analysis of rocks and minerals for major and trace elements on a single low dilution Li-tetraborate fused bead. Adv X-Ray Anal 41:843–867

Kincaid C, Druken KA, Griffiths RW, Stegman DR (2013) Bifurcation of the Yellowstone plume driven by subduction-induced mantle flow. Nat Geosci 6:395–399

Kita NT, Ushikubo T, Fu B, Valley JW (2009) High precision SIMS oxygen isotope analysis and the effect of sample topography. Chemical Geology 264:43–57

Konstantinou A, Valley JW, Strickland A, Miller EL, Fisher C, Vervoort J, Wooden J (2013) Geochemistry and geochronology of the Jim Sage volcanic suite, southern Idaho: implications for Snake River Plain magmatism and its role in the history of Basin and Range extension. Geosphere 9:1681–1703

Lackey JS, Valley JW, Chen JC, Stockli DF (2008) Dynamic Magma Systems, Crustal Recycling, and Alteration in the Central Sierra Nevada Batholith: the Oxygen Isotope Record. J Petrol 49:1397–1426

Larson PB, Taylor HP (1986) An oxygen isotope study of hydrothermal alteration in the Lake City caldera, San Juan Mountains, Colorado. J Volcanol Geoth Res 30:47–82

Leeman WP, Oldow JS, Hart WK (1992) Lithosphere-scale thrusting in the western US Cordillera as constrained by Sr and Nd isotopic transitions in Neogene volcanic rocks. Geology 20:63–66

Leeman WP, Annen C, Dufek J (2008) Snake River Plain - Yellowstone silicic volcanism: implications for magma genesis and magma fluxes. Geological Society of London, Special Publication 304:235–259

Losh S (1997) Stable isotope and modeling studies of fluid-rock interaction associated with the Snake Range and Mormon Peak detachment faults, Nevada. Geol Soc Am Bull 109:300–323

Ludwig KR (2012) Isoplot v. 3.75: A geochronological tool-kit for Microsoft Excel: Special Publication No. 5 Berkley Geochronology Center, Berkeley, 75 pp

MacLeod NS (1989) Geology and mineral resources map of the Sheaville quadrangle, Malheur county, Oregon and Owyhee county, Idaho, State of Oregon Department of Mineral Industries Geological Map Series GMS-64, scale 1:24,000

McCurry M, Rodgers DW (2009) Mass transfer along the Yellowstone hotspot track I: petrologic constraints on the volume of mantle-derived magma. J Volcanol Geoth Res 188:86–98

Monani S, Valley JW (2001) Oxygen isotope ratios of zircon: magma genesis of low $\delta^{18}O$ granites from the British Tertiary Igneous Province, western Scotland. Earth Planet Sci Lett 184:377–392

Morrison J (1994) Meteoric water-rock interaction in the lower plate of the Whipple Mountain metamorphic core complex, California. J Metamorph Geol 12:827–840

Muir-Wood R, King GCP (1993) Hydrological signatures of earthquake strain. J Geophys Res 98(B12):22035–22068

Obrebski M, Allen RM, Xue M, Hung S-H (2010) Slab-plume interaction beneath the Pacific Northwest. Geophys Res Lett 37:1–6

Parsons T, Thompson GA, Smith RP (1998) More than one way to stretch: a tectonic model for extension along the plume track of the Yellowstone hotspot and adjacent Basin and Range Province. Tectonics 17:221–234

Perkins ME, Nash BP (2002) Explosive silicic volcanism of the Yellowstone hotspot: the ash fall tuff record. Geol Soc Am Bull 114:367–381

Pierce KL, Morgan LA (1992) The track of the Yellowstone hot spot: Volcanism, faulting and uplift, *in* Link PK, Kuntz MA, Platt LB, eds., Regional Geology of Eastern Idaho and Western Wyoming. Geological Society of America Memoir 179:1-52

Rodgers DW, McCurry M (2009) Mass transfer along the Yellowstone hotspot track II: kinematic constraints on the volume of mantle-derived magma. J Volcanol Geoth Res 188:99–107

Rodgers DW, Hackett WR, Ore HT (1990) Extension of the Yellowstone plateau, eastern Snake River Plain, and Owyhee plateau. Geology 18:1138–1141

Rodgers DW, Ore TH, Bobo RT, McQuarrie N, Zentner N (2002) Extension and Subsidence of the Eastern Snake River Plain, Idaho, *in* Bonnichsen B, White CM, McCurry M, eds. Tectonic and Magmatic Evolution of the Snake River Plain Volcanic Province. Idaho Geological Survey/University of Idaho, Moscow, United States 30:121-155

Rytuba JJ, Vander Meulen DB, Barlock VE (1991) Tectonic and Stratigraphic controls on Epithermal Precious Metal Mineralization in the Norther Part of the Basin and Range, Oregon, Idaho, and Nevada, *in* Buffa RH, Coyner AR, eds., Geology and Ore Deposits of the Great Basin: Geological Society of Nevada, Reno, Nevada, Fieldtrip Guidebook Compendium 2:636-644

Seligman AN (2012) Generation of low-$\delta^{18}O$ silicic magmas, Bruneau-Jarbidge volcanic center, Yellowstone hotspot: Evidence from zircons, including oxygen isotopes, U-Th-Pb dating, and melt inclusions. MS Thesis, University of Utah

Simakin AG, Bindeman IN (2012) Remelting in caldera and rift environments and the genesis of hot, "recycled" rhyolites. Earth Planet Sci Lett 337–338:224–235

Taylor HP (1986) Igneous rocks: iI. Isotopic Case Studies of Circumpacific Magmatism. Rev Mineral 16:273–317

Taylor HP, Sheppard SMF (1986) Igneous rocks: i. Processes of Isotopic Fractionation and Isotope Systematics, Reviews in Mineralogy 16:227–271

Valley JW (1986) Stable Isotope Geochemistry of Metamorphic Rocks. Rev Mineral 16:445–489

Valley JW (2003) Oxygen isotopes in zircon. Rev Mineral Geochem 53:343–385

Valley JW, Chiarenzelli JR, McLelland JM (1994) Oxygen isotope geochemistry of zircon. Earth Planet Sci Lett 126:187–206

Valley JW, Kitchen N, Kohn MJ, Niendorf CR, Spicuzza MJ (1995) UWG-2, a garnet standard for oxygen isotope ratios: strategies for high precision and accuracy with laser heating. Geochim Cosmochim Acta 59:5223–5231

Valley JW, Bindeman IN, Peck WH (2003) Empirical calibration of oxygen isotope fractionation in zircon. Geochim Cosmochim Acta 67:3257–3266

Valley JW, Lackey JS, Cavosie AJ, Clechenko CC, Spicuzza MJ, Basei MAS, Bindeman IN et al (2005) 4.4 billion years of crustal maturation: oxygen isotope ratios of magmatic zircon. Contrib Miner Petrol 150:561–580

Vander Meulen DB (1989) Intracaldera tuffs and central-vent intrusion of the Mahogany Mountain Caldera, Eastern Oregon, U.S. Geological Survey, OFR 89-77

Vander Meulen DM, Rytuba JJ, Grubensky MJ, Goeldner CS (1987) Geologic Map of the Bannock Ridge Quadrangle, Malheur County, Oregon, U.S. Geological Survey, MF-1903, scale 1:24,000

Vander Meulen DB, Rytuba JJ, Vercoutere TL, Minor SA (1987) Geologic Map of the Rooster Comb Quadrangle, Malheur County, Oregon, U.S. Geological Survey, MF-1902, scale 1:24,000

Vander Meulen DM, Rytuba JJ, Minor SA, Harwood CS (1989) Preliminary Geologic map of the Three Fingers Rock Quadrangle, Malheur County, Oregon, U.S. Geological Survey OFR 89-344, scale 1:24,000

Wang X-C, Li Z-X, Li X-H, Li Q-L, Tang G-Q, Zhang Q-R, Liu Y (2011) Non glacial origin for low-$\delta^{18}O$ Neoproterozoic magmas in the South China Block: evidence from new in situ oxygen isotope analyses using SIMS. Geology 39:735–738

Watts KE, Leeman WP, Bindeman IN, Larson PB (2010) Supereruptions of the Snake River Plain: two-stage derivation of low-$\delta^{18}O$ rhyolites from normal-$\delta^{18}O$ crust as constrained by Archean xenoliths. Geology 38:503–506

Watts KE, Bindeman IN, Schmitt AK (2011) Large-volume Rhyolite Genesis in Caldera Complexes of the Snake River Plain: insights from the Kilgore Tuff of the Heise Volcanic Field, Idaho, with Comparison to Yellowstone and Bruneau-Jarbidge Rhyolites. J Petrol 52:857–890

Watts KE, Bindeman IN, Schmitt AK (2012) Crystal scale anatomy of a dying supervolcano: an isotope and geochronology study of individual phenocrysts from voluminous rhyolites of the Yellowstone caldera. Contrib Miner Petrol 164:45–67

Whittington AG, Hofmeister AM, Nabelek PI (2009) Temperature-dependent thermal diffusivity of the Earth's crust and implications for magmatism. Nature 458:319–321

Wotzlaw J, Bindeman IN, Watts KE, Schmitt AK, Caricchi L, Schaltegger U (2014) Linking rapid magma reservoir assembly and eruption trigger mechanisms at evolved Yellowstone-type supervolcanoes. Geology 42:807–810

Zilberfarb AR, Lackey JS, Sendek CL, Eisenberg JL, Murphy BS, Ferguson LA, Raschick NA, Simpson ND, Bindeman IN (2012) Variable recycling of anomalous low-$\delta^{18}O$ Proterozoic crust in the Ord Mountains, Mojave Desert, CA. Geological Society of America Abstracts with Programs 44(7):281